Energy Technology
Generation, Conversion, Storage, Distribution

RESEARCH ARTICLE OPEN ACCESS

Advanced Virtual Impedance for Power-Sharing Improvement in Microgrids Using Different SOGI Methods: A Comparative Study

Camelia Ait Hammouda[1] | Abdellah Benallal[2] | Rafik Bradai[1] | Adrian Ilinca[3]

[1]LATSI Laboratory of Blida 1 University, Blida, Algeria | [2]Department of Engineering, Université du Québec à Rimouski, Rimouski, Quebec, Canada | [3]Mechanical Engineering Department, Ecole de Technologie Supérieure, Montreal, Quebec, Canada

Correspondence: Adrian Ilinca (adrian.ilinca@etsmtl.ca)

Received: 13 August 2025 | **Revised:** 21 November 2025 | **Accepted:** 7 December 2025

Keywords: droop control | microgrid | power sharing | three-phase voltage source inverters | virtual impedance control

ABSTRACT

The droop control strategy is necessary for the operation of a microgrid (MG) to control power sharing among parallel-connected distributed generations (DGs). However, the main drawback of this control strategy is poor power sharing due to line impedance mismatch. To overcome this, the virtual impedance (VI) control concept is adopted as a practical solution and effective enhancement to improve power sharing. Despite this improvement, conventional VI-based methods still face challenges in harmonic power sharing under nonlinear load conditions. This article proposes an advanced VI-based control scheme for three-phase voltage source inverters (VSIs) forming a stand-alone MG. It is designed using the second-order generalized integrator (SOGI) method and its variants—ESOGI, MSOGI, and DSOGI—to accurately estimate and compensate for harmonic components in the $\alpha\beta$ reference frame. Therefore, improvements in both power and harmonic sharing are expected. To this end, a detailed structural relationship among the different SOGI variants is identified and then compared using a testbed consisting of three DG-based MG simulated in MATLAB/Simulink. Results demonstrate that the proposed approach significantly improves performance, reducing total harmonic distortion (THD) from 5.2% with the classical SOGI to 1.9% with the DSOGI, and decreasing power-sharing error from 7.8% to 1.2%, confirming its effectiveness under various operating conditions. Each variant exhibits specific advantages and limitations.

1 | Introduction

The concept of microgrids (MGs) based on distributed energy resources (DERs) has emerged as an attractive solution for integrating renewable energy sources (RES) into modern power systems. MGs can operate in both grid-connected and islanded modes [1, 2]. In islanded operation, the primary control layer, typically implemented using droop control, maintains load sharing among distributed generation (DG) units and ensures stable frequency and voltage amplitude within the MG [3, 4]. Droop control enables DG units to cooperatively share active and reactive power in response to load changes by adjusting their voltage and frequency. However, a key limitation of this method is its inability to ensure accurate reactive power sharing and proper harmonic current distribution when DG line impedances are mismatched. To address this issue, the virtual impedance (VI) concept has been introduced to improve harmonic current sharing, enhance reactive power-sharing accuracy, and increase MG stability [5].

Various control approaches have been proposed in the literature for three-phase MGs [6–11], providing valuable insights into improving system performance. A classical method—multiplying the current derivative by an inductance—has been widely applied to three-phase voltage source inverters (VSIs) to enhance reactive power sharing among DERs. Buraimoh and Davidson [12] investigated the impact of different VI parameter values

on overall MG performance. Other studies [3, 13–16] applied the VI concept to address power decoupling and sharing challenges by increasing the effective line impedance between inverters and the common bus. He and Li [17] offered a detailed design, analysis, and implementation framework for VI-based control in DG applications within MGs. Additional works [18–20] employed VI-based schemes to further enhance power-sharing capabilities.

Recent developments have introduced adaptive VI control methods, including communication-based [21], consensus-based [22], and sliding-mode-based [23] approaches, aimed at achieving accurate harmonic power sharing and voltage harmonic compensation in islanded MGs. At the distributed control level, the strategy in [24] enables robust power sharing while maximizing feeder power transfer capacity. The influence of communication delays and failures on MG performance has also been extensively analyzed in [25]. To improve reactive power sharing under unbalanced conditions, researchers have proposed solutions such as active power filters (APFs) [26] and voltage compensation methods [27, 28]. Ko et al. [29] further introduced a dynamic virtual inductance loop to compensate for voltage drops caused by line impedance.

Another approach to implementing VI involves the use of the second-order generalized integrator (SOGI) strategy, which has been further developed in [30, 31]. SOGI is primarily employed to extract the fundamental components of grid signals and track frequency variations. Over time, several enhanced variants have been introduced to improve performance in complex operating environments and under distorted or dynamic conditions. These include the enhanced SOGI (ESOGI) [32, 33] and the high-order generalized integrator (HOGI) [34, 35], both of which address power quality issues more effectively. Additional techniques discussed in the literature [36], such as TOGI, DOGI, and n-SOGI, aim to mitigate output distortions at selected harmonic frequencies caused by noise and nonlinear loads, ultimately improving total harmonic sistortion (THD) performance.

Despite these advancements, most existing studies focus primarily on signal filtering and frequency tracking, without fully integrating SOGI-based methods into VI control strategies for power sharing in MGs under harmonic distortion and nonlinear load conditions. For example, the standard SOGI is widely adopted for its simplicity and ease of implementation, especially for extracting the fundamental frequency component from distorted grid signals—an essential step for phase-locked loops (PLLs) and grid synchronization. However, its performance deteriorates when higher order harmonics are present, limiting its effectiveness in systems with strong nonlinear loads. Enhancements such as ESOGI have been proposed to improve harmonic suppression by modifying the internal feedback loop. While these modifications generally enhance selectivity and responsiveness, their integration into VI loops remains rare in the literature, with most applications focusing on voltage estimation or frequency tracking rather than harmonic current management in decentralized MGs.

More advanced variants—such as DSOGI, TSOGI, MSOGI, and n-SOGI—enable simultaneous tracking of multiple harmonics, offering significant potential for harmonic compensation. Nevertheless, their evaluation within a VI framework, particularly their impact on power-sharing dynamics, remains limited. Similarly, HOGI, designed for robust operation in noisy or highly distorted environments, is typically evaluated in signal analysis studies rather than in real-time control scenarios involving DG.

A further shortcoming in the literature is the lack of comparative analyses of these methods when integrated into practical control strategies. While numerous studies report performance metrics such as THD reduction or estimation error, very few investigate their influence on power sharing, voltage regulation, or system stability under realistic MG operating conditions. Consequently, there is currently no clear guideline on selecting the most suitable SOGI-based method for deployment in MG systems using a virtual impedance control loop (VICL).

In this context, the present article seeks to address the identified research gap by implementing and comparatively evaluating several SOGI variants within a VI-based power-sharing framework for three-phase droop-controlled VSIs operating in parallel in an islanded MG. It represents the first comparative evaluation of SOGI, ESOGI, MSOGI, and DSOGI within a VICL, analyzing their performance–complexity trade-offs under realistic MG operating scenarios. The central objective is to demonstrate that accurate estimation of the fundamental and harmonic components of the current—required for computing the VI output voltage—enables precise control of the VI output, thereby reducing circulating currents. By doing so, the proposed VICL is expected to enhance the accuracy of active, reactive, and harmonic power sharing among DG units. Other SOGI extensions, such as TOGI, DOGI, TSOGI, and HOGI, were excluded from this research paper due to their greater computational complexity and reduced suitability for real-time VICL applications.

To validate the proposed approach, a MATLAB/Simulink testbed of an MG comprising three parallel-connected inverters is developed and tested under a variety of operating cases. The simulation results confirm the high accuracy of active and reactive power sharing, as well as improved harmonic compensation, across different load and network conditions. This study contributes to the field by facilitating both the analysis and optimization of VICL designs based on SOGI variants, ultimately improving overall MG performance.

The remainder of this aticle is organized as follows: Section 2 reviews the primary control of a three-phase VSI in an MG, including its operating principles, cascaded inner control loops, the mathematical foundations of droop control, and the design of a VI-based power-sharing scheme. Section 3 details the proposed VICL approach using SOGI variants, including its structure and key formulations. Section 4 presents and discusses the simulation results. Section 5 concludes the article with the main findings and implications of the research.

2 | Materials and Methods

2.1 | Proposed Scheme of Three-Phase VSIs' Power-Sharing Control

In MGs, the primary control level is the lowest in the hierarchy. Its primary role is to manage sudden changes in power load, whether linear or nonlinear [37]. This control is local and decentralized, meaning it relies solely on local measurements, with each inverter having its dedicated control stage, enabling each DG unit to function independently without communication during regular operation. It plays a crucial role in guaranteeing the reliability of the MG and enhancing its overall performance and

stability. It adjusts the frequency and voltage outputs of inverters to serve as a reference for the inner multiloop controller. This helps reduce circulating currents that can occur when multiple converters are connected in parallel. Additionally, it ensures the precise sharing of active and reactive power among these converters. It can function in both grid-connected and autonomous modes, with a seamless transition between them.

The control structure for this level, based on a single inverter unit, intended for the three-phase VSIs, is shown in Figure 1. The power stage of a DG unit consists of a DC source supplying an inverter with an LC filter linked to the point of common coupling (PCC) through an impedance line. This setup comprises two key components:

a) The cascaded inner loop that comprises the current control loop (CCL) and voltage control loop (VCL), which are responsible for stabilizing the inverter voltage frequency and amplitude.

b) The external power control loop is based on the droop control method, along with a VI loop and a power calculation block. Meanwhile, droop control controls the active and reactive power output of the DG.

As depicted in Figure 1, before droop control was implemented, the power calculation stage used the filter output currents and voltages, transformed into the $\alpha\beta$ frame and detected by the SOGI-frequency locked loop (SOGI-FLL), to compute the average real and reactive power.

To address mismatched inductive/resistive feeder impedance, the optional VI loop improves power quality and power-sharing accuracy within the MG [38].

Further details about these components will be elaborated upon in the subsequent sections.

2.2 | Power Calculation Block

Adding the power calculation component to the main control setup is vital for determining the average levels of active (P_i) and reactive (Q_i) powers. Generally, when dealing with three-phase MGs, they can easily be calculated by converting the three-phase voltages and currents (in *abc* frame) to the $\alpha\beta$ (or *dq*) reference frame. This involves applying established equations, such as in Equation (1), as appropriate.

$$\left\{\begin{array}{l} P_i = \left(v_{c\cdot\alpha} \times i_{L_2\cdot\alpha} + v_{C\cdot\beta} \times i_{L_2\cdot\beta}\right) \\ Q_i = \left(v_{C\cdot\beta} \times i_{L_2\cdot\alpha} - v_{C\cdot\alpha} \times i_{L_2\cdot\beta}\right) \end{array}\right\} \quad \left\{\begin{array}{l} P_i = \left(v_{C\cdot d} \times i_{L_2\cdot d} + v_{C\cdot q} \times i_{L_2\cdot q}\right) \\ Q_i = \left(v_{C\cdot q} \times i_{L_2\cdot d} - v_{C\cdot d} \times i_{L_2\cdot q}\right) \end{array}\right\} \tag{1}$$

where $v_{C\cdot\alpha\beta}(v_{C\cdot dq})$ and $i_{L1\cdot\alpha\beta}(i_{L1\cdot dq})$ essentially stand for the in-phase and quadrature-phase aspects of both the inverter's output voltage and current.

Figure 2 illustrates the schematic designs for the power calculations for three-phase systems. After determining the instantaneous active and reactive powers, the data are processed with a low-pass filter (LPF) to obtain the corresponding average values.

The LPF's transfer function ($G_{\mathrm{LPF}}(s)$) can be described as follows in the *s*-domain:

$$G_{\mathrm{LPF}}(s) = \frac{\omega_{\mathrm{cutt\cdot off}}}{s + \omega_{\mathrm{cutt\cdot off}}} \tag{2}$$

$\omega_{\mathrm{cutt\cdot off}}$ in this context is the LPF's cutoff frequency. Usually, it is set to a relatively low value to remove any underlying harmonic components [39].

2.2.1 | Droop Control Strategy

In AC MGs with multiple DG systems operating in parallel, ensuring optimal power sharing is complex. The goal is to allocate each DG its share of active and reactive power, meeting the

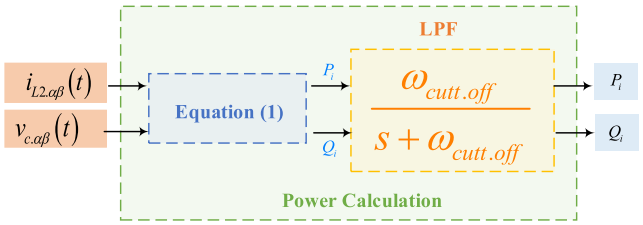

FIGURE 2 | Power calculation block diagram.

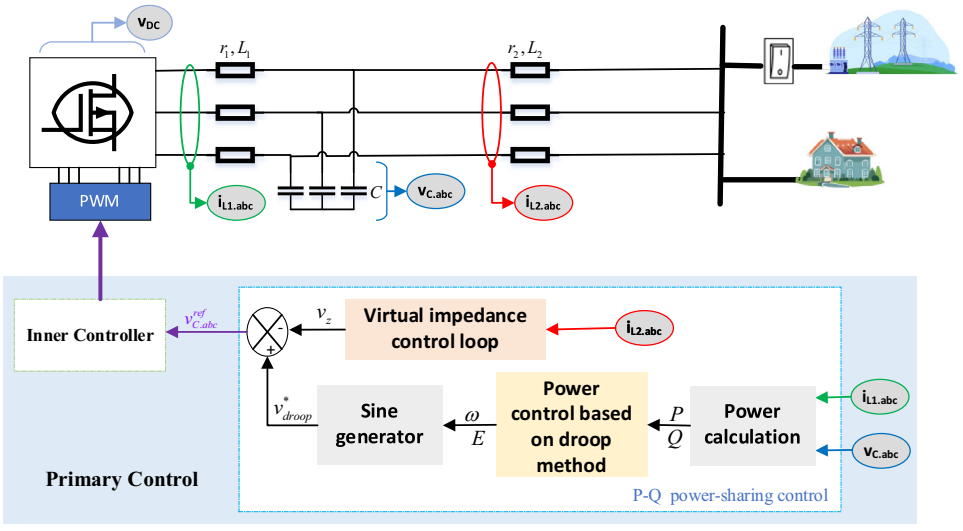

FIGURE 1 | Primary control configuration.

overall load demand without overloading any particular DER. This should also maintain stable voltage and frequency levels, thus upholding MG stability.

In MG literature, centralized architectures are often considered to enhance power sharing due to their accuracy and reduced voltage and frequency deviations. Two common centralized power-sharing strategies are the master–slave approach [40, 41] and concentration methods [42].

Additionally, there is a preference for controlling numerous parallel VSIs, while preventing the circulation of current among them [3, 43–45], in a distributed manner using droop control, considered as the heart of the primary control [1, 43, 46–49]. This approach demands less external communication, relies on local measurements, and offers flexibility for various plug-and-play MG devices [3, 50–54]. Droop control is based on the principle of power flow in traditional power systems with parallel synchronous generators, which distribute any load increases based on their rated capacities. When there is a sudden surge in power demand, it can be offset by the mechanical power of the rotor. This same concept is used in exciter control of synchronous machines, where the voltage decreases as reactive power increases. These principles are integrated into power electronic MGs via droop functions [55–58]. The droop control operates within a range of 100 ms to 1 s. It assigns individual frequency and voltage setpoints to each inverter based on power-sharing needs. While effective in maintaining stability and power balance, it has limitations concerning voltage regulation and harmonic compensation. Various control schemes and configurations of droop control exist to enable efficient power sharing for both linear and nonlinear loads.

The conventional droop control, often referred to as $P-\omega$ and $Q-E$ droops, uses the active p/frequency (P/f) and reactive power/voltage (Q/V) controls to realize decoupling control of active and reactive power. A comprehensive review of droop control strategies is summarized in [59].

However, DG systems often have different output impedances, requiring specific adaptations to droop control. They can be resistive (R/*inverters*), capacitive (C/*inverters*), resistive–capacitive (RC/*inverters*), or resistive–inductive (RL/*inverters*). The literature reports that it is not feasible to operate an inverter with an inductive output in parallel with another inverter with a capacitive output. In most cases, the output impedance is inductive (L/*inverters*), especially around the fundamental frequency. Nonetheless, for low-voltage MGs, where the equivalent impedance between any two DG systems can be either resistive or inductive (with a DG coupling transformer or a grid-side inductor), the impedance resistance R becomes essential and cannot be neglected.

This mechanism ensures that DG units distribute the workload by adjusting each VSI's frequency based on the supplied real power. Consequently, each generator adjusts to variations in the overall load while adhering to its distinctive frequency droop characteristic, all without the need for interunit communication. Similarly, a reduction in voltage amplitude (E) coupled with reactive power (Q) facilitates equitable reactive power sharing.

In the droop control loop, the frequency (ω) and voltage amplitude (E) of the inverter output are set based on the average active power (P) and reactive power (Q) supplied by the VSI to the MG. To put it in simpler terms, these connections can be articulated as follows:

$$\begin{cases} \omega_i = \omega^* + m(P^* - P) \\ E_i = E^* + n(Q^* - Q) \end{cases} \tag{3}$$

Here, ω^* and E^* refer to the frequency and amplitude of the output voltage when there is no load. P^* and Q^* represent the reference for active and reactive power, and during island operation mode [1], these references are set to zero.

The control parameters, represented by n and m, are linked to the inclines of the frequency and amplitude functions. These figures are based on the allowed frequency and voltage deviations ($\Delta\omega$ and ΔE), as well as the maximum active and reactive powers ($P_{\max}$ and $Q_{\max}$), respectively. This relationship can be expressed as follows:

$$m = \frac{\Delta\omega}{P_{\max}},\ n = \frac{\Delta E}{Q_{\max}} \tag{4}$$

Figure 3 represents the droop control loop block design. As shown, a sinusoidal signal generator receives the frequency and voltage produced by the droop controller. This generator produces the reference output voltage ($v^*_{\text{droop}}(t)$) for the VSI. The following equation can express the relationship governing this:

$$v^*_{\text{droop}}(t) = E_i \times \sin\left(\omega_i \times t\left[0\ \frac{2\pi}{3}\ -\frac{2\pi}{3}\right]^T\right) \tag{5}$$

The voltage reference from the droop control is then directed to the inputs of the inner voltage and current control loops.

Figure 4 provides a visual representation of the droop control characteristics for two VSIs. It can be observed that the droop slopes play a role as a negative correlation between P/Q and ω/E, respectively. It is important to note that in steady-state conditions, the frequency and amplitude match in both VSIs, and the same slope parameters align, indicating that $n_1 = n_2$ and $m_1 = m_2$. This synchronization ensures that the two DG units achieve effective and balanced active and reactive power sharing.

To derive the droop functions, we should analyze the equivalent circuit of two VSIs connected in parallel to an AC bus via line impedances as given in Figure 5. In this figure, each inverter stage is modeled as a sinusoidal voltage source with an output impedance in series. According to this figure, the expression

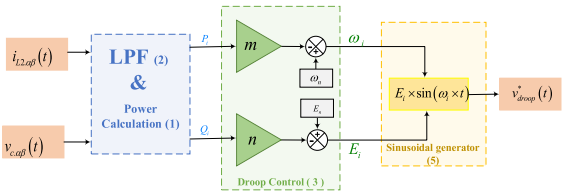

FIGURE 3 | Droop control schematic diagram.

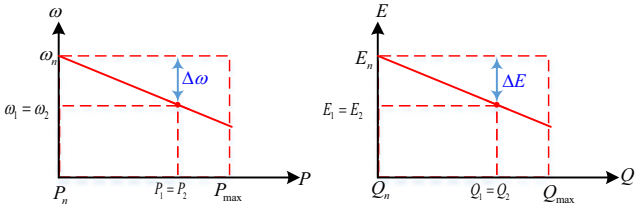

FIGURE 4 | Droop control characteristics.

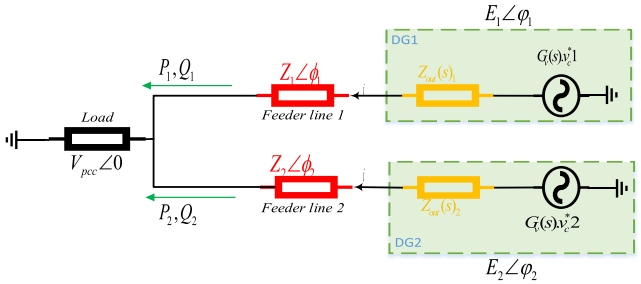

FIGURE 5 | Equivalent electric circuit of two paralleled VSIs.

of the active P and reactive Q power of each DG, after some mathematical manipulation, can be obtained as follows:

$$\begin{cases} P_i = \dfrac{3V_{\mathrm{PCC}}}{Z_i}\left(\left(E_i\cos\left(\varphi_i\right) - V_{\mathrm{PCC}}\right)\cos\left(\phi_i\right) + E_i\sin\left(\varphi_i\right)\sin\left(\phi_i\right)\right) \\ Q_i = \dfrac{3V_{\mathrm{PCC}}}{Z_i}\left(\left(E_i\cos\left(\varphi_i\right) - V_{\mathrm{PCC}}\right)\sin\left(\phi_i\right) - E_i\sin\left(\varphi_i\right)\cos\left(\phi_i\right)\right) \end{cases} \tag{6}$$

where $E_i\angle\varphi_i$ is the inverter output voltage, $E_{\mathrm{pcc}}\angle 0$ is the voltage at the PCC, and $Z_i\angle\phi_i = R_i + jX_i$ is the inverter to the PCC bus impedance, which considers the inverter output impedance and the line impedance of the connection wires.

By assuming that the phase difference between the inverters' output voltages and the PCC is very small ($\varphi_i \ll 1 \rightarrow \sin\varphi_i = \varphi_i$ and $\cos\varphi_i = 0$), Equation ((6)) yields:

$$\begin{cases} P_i = \dfrac{V_{\mathrm{PCC}}}{Z_i}\left(\left(E_i - V_{\mathrm{PCC}}\right)\cos\left(\phi_i\right) + E_i\varphi_i\sin\left(\phi_i\right)\right) \\ Q_i = \dfrac{V_{\mathrm{PCC}}}{Z_i}\left(\left(E_i - V_{\mathrm{PCC}}\right)\sin\left(\phi_i\right) - E_i\varphi_i\cos\left(\phi_i\right)\right) \end{cases} \tag{7}$$

Based on the line impedance nature, the expression of the active and reactive powers can be defined as follows:

For pure inductive line impedance, i.e., $X_i \gg R_i$ ($\rightarrow Z_i\angle\phi_i \cong X_i\angle\frac{\pi}{2}$):

$$\begin{cases} P_i = \dfrac{E_iV_{\mathrm{PCC}}}{X_i}\varphi_i \\ Q_i = \dfrac{\left(E_i - V_{\mathrm{PCC}}\right)V_{\mathrm{PCC}}}{X_i} \end{cases} \tag{8}$$

For pure resistive line impedance, i.e., $X_i \ll R_i$ ($\rightarrow Z_i\angle\phi_i \cong R_i\angle 0$):

$$\begin{cases} P_i = \dfrac{\left(E_i - V_{\mathrm{PCC}}\right)V_{\mathrm{PCC}}}{R_i} \\ Q_i = \dfrac{-E_iV_{\mathrm{PCC}}}{R_i}\varphi_i \end{cases} \tag{9}$$

where X_i and R_i are the reactance and resistance of the inverter output impedance.

It can be seen that, for pure inductive impedance, the active power depends on the phase angle Equation (8) and the reactive power depends on the voltage Equation (9). In the case of pure resistive impedance, the f/Q and V/P characteristics seen in the previous chapter are found.

Based on the characteristics, the expressions of the droop controller can be formulated as follows:

- Pure inductive impedance:

$$\begin{cases} \omega_i = \omega^* - \left(\dfrac{\omega_{\mathrm{f}}}{s+\omega_{\mathrm{f}}}\right)nP_i \\ E_i = E^* - \left(\dfrac{\omega_{\mathrm{f}}}{s+\omega_{\mathrm{f}}}\right)mQ_i \end{cases} \tag{10}$$

- Pure resistive impedance:

$$\begin{cases} E_i = E^* - \left(\dfrac{\omega_{\mathrm{f}}}{s+\omega_{\mathrm{f}}}\right)nP_i \\ \omega_i = \omega^* - \left(\frac{\omega_{\mathrm{f}}}{s+\omega_{\mathrm{f}}}\right)mQ_i \end{cases} \tag{11}$$

where ω^* and E^* correspond to the nominal frequency and amplitude of the output voltage at no load. n and m are the frequency and amplitude droop gains, which can be determined by the maximum frequency and voltage deviations ($\Delta f_{\max}$ and $\Delta V_{\max}$) divided by the inverter active and reactive rated power, and the first-order transfer function is the transfer function of the LPF with a cutoff frequency ω_{f}.

It is worth noting that this study assumes purely inductive feeder impedances to simplify the control analysis and highlight the impact of SOGI-based VI schemes. In practical MGs, however, feeder lines typically exhibit mixed R–L characteristics, where both resistive and inductive components influence active and reactive power coupling. In such cases, modified droop coefficients or impedance-compensation strategies can be used to maintain accurate power sharing.

The droop control method discussed earlier plays a crucial role in MG operation, particularly in islanded mode. However, despite its effectiveness in balancing the distribution of active and reactive power, it faces challenges with current sharing. This is because the inverters' output current depends on their output impedance ratios. Additionally, harmonic currents can induce voltage distortion at the PCC, especially when VSIs power nonlinear loads.

To address these limitations and improve power-sharing accuracy, droop coefficients are compensated [60] and tuned [61]. In addition, researchers have explored advanced control strategies, including model predictive control (MPC), sliding mode control (SMC), and VICL. MPC uses a mathematical model to optimize control actions while accounting for system dynamics and constraints. SMC provides robustness against uncertainties and disturbances, ensuring precise voltage and frequency regulation. VI control employs VIs to mimic the behavior of a resistive network, improving voltage regulation and damping low-frequency oscillations, thereby ensuring precise sharing of current-harmonic components when DG units supply power to nonlinear loads.

2.2.2 | VI Loop

As mentioned earlier, despite the effectiveness of the primary control approach based on this technique in achieving an average power distribution, it does have certain limitations regarding proper reactive power and harmonic sharing [62–64] due to mismatches in the DGs' line impedances. The droop control method is not well suited for distributing current harmonics, mainly when VSIs supply power to nonlinear loads. Consequently,

advancements in droop control aim to enhance the precision of harmonic sharing [58]. In this regard, the VICL concept has been adopted to achieve more accurate harmonic-current sharing, improve the reactive power-sharing accuracy, and enhance MG stability by standardizing their output impedance [65, 66].

Various approaches have been explored in the literature for three-phase MGs [3, 13–16], offering valuable insights into their control and performance enhancement. The classical method involves multiplying the current derivative by an inductance and has been widely adopted in three-phase VSIs. This control approach has enhanced reactive power sharing among DERs.

This virtual output impedance loop incorporates a fast control loop that derives a pure inductive equivalent impedance. This impedance is formed by the series connection of the MG impedances as perceived by the VSI, along with the VI, as shown in Figure 1, which illustrates the equivalent circuit of VSIs with line and VIs. The process of establishing this virtual output impedance involves adjusting the output-voltage reference in proportion to the time derivative of the inverter output current. This adjustment increases the inverter's output inductive impedance, which, in turn, raises the impedance between the VSI and the standard bus line. Consequently, it reduces the circulating current within the MG. The expression for implementing this virtual inductive output impedance can be stated as follows [30]:

$$Z_{\mathrm{v}}(s) = s \cdot L_{\mathrm{v}} \tag{12}$$

Here, L_{v} represents the inductor value of the virtual output impedance, and s is the Laplace operator.

Figure 1 illustrates the block diagram of the programmed droop control scheme based on virtual output impedance. In this setup, a VI unit calculates the voltage of the virtual output impedance, taking the inverter output current as input. This VI voltage is subsequently incorporated as an additional element in the output voltage reference, seamlessly provided by the droop control loop, as depicted below:

$$v_{\mathrm{C}}^{*}(s) = v_{\mathrm{droop}}^{*}(s) - Z_{\mathrm{v}}(s) i_{L2}(s) \tag{13}$$

The equation above provides the updated output-voltage reference incorporating the virtual output impedance. In fact, each inverter's control loop includes a similar loop.

It is important to note that when the virtual output impedance is programmed as the time derivative of the inverter current, the system becomes highly responsive to output current noise and to nonlinear loads with slow rate-of-change. In response to this challenge, an implementation of the VI based on the SOGI-quadrature signal generator (SOGI-QSG) scheme has been proposed in the literature, as depicted in Figure 6 [30]. This implementation capitalizes on the SOGI method's features to establish a VI control scheme offering several advantages: i) reduced sensitivity to output current noise; ii) elimination of the need for time derivative calculations; iii) improved THD of the output voltage, and iv) enhanced handling of nonlinear loads [39]. This concept seamlessly integrates into our hierarchical control scheme, where the SOGI-FLL scheme becomes an integral part of all three control levels.

2.2.3 | Inner Control Loops

Level zero, or the inner control loop, also known as the low-level voltage and current controller, establishes the operational state of the DG units. It plays a crucial role in maintaining stable control of the inverter's output voltage and current, even in the presence of disturbances. This objective is accomplished by adjusting the inverter's output voltage to match the desired reference value.

Figure 7a shows the schematic diagram of the inner controller for VSIs, which typically consists of an outer VCL and an internal CCL. These two control loops work together to regulate the inverter's output voltage and control the current, maintaining system stability with high bandwidth and performance, ensuring rapid response across various operating conditions. The inner controller provides the duty cycle to the sinusoidal pulse width modulator (PWM), which, in turn, dictates the gating signals for the IGBTs in the VSI. For more detailed insights into this control level, refer to [8, 9].

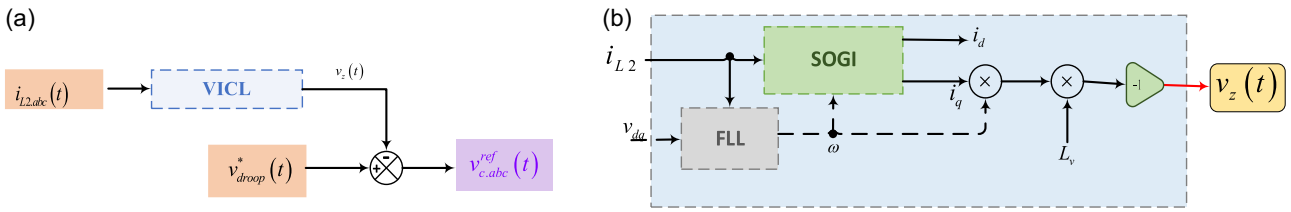

FIGURE 6 | (a) VI-based reference generation and (b) implementation using the SOGI approach.

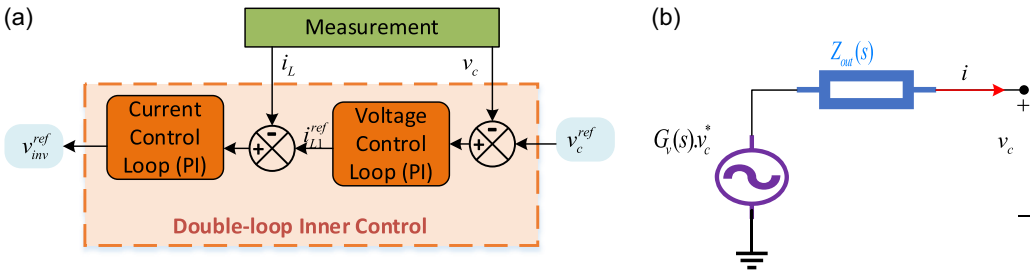

FIGURE 7 | Block diagram of (a) the inner control loop and (b) the equivalent circuit.

In a three-phase system, the inner control loop design is essential for the MG performance. Recently, proportional resonant (PR) controllers have been developed to alleviate tracking uncertainty in some control approaches and to provide independent voltage control for grid-forming VSIs. Additionally, in the presence of nonlinear loads, they have significantly reduced THD by allowing for selective harmonic rejection. The fundamental drawback of this controller is its sensitivity to phase and frequency changes in the provided signals [67–69]. Model predictive controllers (MPCs) have been introduced to improve VSI control performance [70]. The MPC uses a model of the system to predict its operation; thus, variations in system parameters reduce the control system's effectiveness. The neural network and fuzzy controllers are popular intelligence-based control methods proposed in the literature, aiming to cope with system parameter deviations without requiring a precise mathematical model of the system. Except that training these approaches is not easy. Besides, the repetitive-based control strategy performs admirably in the presence of nonlinear loads by reducing output voltage and current THD; however, it suffers from poor tracking accuracy and dynamic performance, and it requires more memory than other strategies.

Sliding-mode control [71] is also proposed for controlling VSIs; it provides a fast time response and strong tolerance to fluctuations in VSI and filter parameters. This approach, on the other hand, is highly sensitive to load fluctuations and exhibits poor steady-state tracking. Another conventional control strategy that is gaining much attention is a simple proportional–integral (PI) controller [72], which ensures fast time response with minimal steady-state tracking error. PI regulators are commonly proposed in both the $\alpha\beta$ and the dq frames to independently regulate active and reactive power. By designing separate PI controllers for the d-axis and q-axis variables, independent regulation of voltage and frequency can be achieved.

The inner controller introduced in this study is a double-loop scheme that is composed of an outer VCL and an internal CCL. They are based on PI regulators, and their corresponding closed-loop transfer functions are expressed as follows:

$$\begin{cases} G^{\mathrm{BF}}_{v\cdot dq}(s) = \dfrac{v_{\mathrm{C}\cdot dq}}{v_{\mathrm{C}\cdot \mathrm{ref}\cdot dq}} = \dfrac{1}{C}\dfrac{k_{p\cdot v}s + k_{i\cdot v}}{s^2 + \left(\frac{k_{p\cdot v}}{C}\right)s + \frac{k_{i\cdot v}}{C}} \\ G^{\mathrm{BF}}_{i\cdot dq}(s) = \dfrac{i_{L1\cdot dq}}{i_{L1\cdot \mathrm{ref}\cdot dq}} = \dfrac{1}{L_1}\dfrac{k_{p.i}s + k_{i.i}}{s^2 + \left(\frac{r_1 + k_{p\cdot i}}{L_1}\right)s + \frac{k_{i.i}}{L_1}} \end{cases} \tag{14}$$

where $k_{p.i}$, $k_{p.v}$, $k_{i.i}$, and $k_{i.v}$ are the proportional and integral gains of current and voltage controllers, respectively.

By matching Equation (14) to the desired transfer functions in Equation (15) below, the controllers' gains can be determined.

$$\begin{cases} G^{\mathrm{FB}}_{i\cdot dq}(s) = \dfrac{\omega_i^2}{s^2 + 2\zeta_i\omega_i s + \omega_i^2} \\ G^{\mathrm{FB}}_{v\cdot dq}(s) = \dfrac{\omega_v^2}{s^2 + 2\zeta_v\omega_v s + \omega_v^2} \end{cases} \tag{15}$$

Note that the parameters $\zeta_i, \omega_i, \zeta_v$, and ω_v are precisely obtained from the transient response overshoot $M_{p.i}$, $M_{p.v}$, and settling time $T_{s.i}$, $T_{p.v}$ expressed by:

$$M_{p.i} = e^{\frac{\zeta_i\pi}{\sqrt{1-\zeta_i^2}}}, T_{s\cdot i} = \frac{4}{\zeta_i\omega_i}, M_{p\cdot v} = e^{\frac{\zeta_v\pi}{\sqrt{1-\zeta_v^2}}}, T_{s\cdot v} = \frac{4}{\zeta_v\omega_v} \tag{16}$$

More details on the inner controller can be found in [73], while the droop control and the proposed VICL are discussed in the following section.

2.3 | SOGI-Based VICLs Presentation

It is worth mentioning that each SOGI variant is integrated into the VICL as a harmonic estimation stage. Its $\alpha\beta$ output signals modulate the VI voltage reference, directly affecting voltage compensation and harmonic current sharing.

In addition, in most research articles, the $\alpha\beta$ frame was selected over dq due to its more straightforward implementation and better suitability for harmonic detection and multifrequency estimation within VICL.

2.3.1 | Classical SOGI

The SOGI is a signal-processing method widely used for filtering and extracting the fundamental component of an input signal, particularly in grid synchronization applications such as phase-locked loops (PLLs). Its basic structure is depicted in Figure 8.

Here, $v_{c\text{-}\alpha\beta}$ are defined as generated orthogonal output signals, $v_{c\text{-}a}$ is the input signal of the a-phase, ω is the fundamental frequency generated by the droop control, and k is the proportional gain chosen as a trade-off between time response and filtering performances. The dynamic behavior of the SOGI can be expressed as a second-order system whose damping ratio ξ is approximately

$$\xi \approx \frac{k}{2}$$

A classical design choice for grid synchronization and harmonic extraction applications is $\xi = 1/\sqrt{2} \approx 0.707$, which ensures minimal overshoot and a good compromise between settling time and harmonic rejection. This leads naturally to $k \approx \sqrt{2} \approx 1.414$, consistent with widely adopted tuning rules in [74–76]. In our design, $k = 1.4$ was retained because it preserves selectivity around the fundamental frequency, improves rejection of the 5th, 7th, and 11th harmonics when used inside the VICL, and ensures a settling time of 8–10 ms for the $\alpha\beta$ components, satisfying the MG primary-control timing constraints.

As shown in Figure 8, the SOGI operates as a quadrature signal generator, producing two orthogonal signals from a single-phase input while dynamically adjusting to track the fundamental frequency and attenuate harmonics. Mathematically, it is modeled

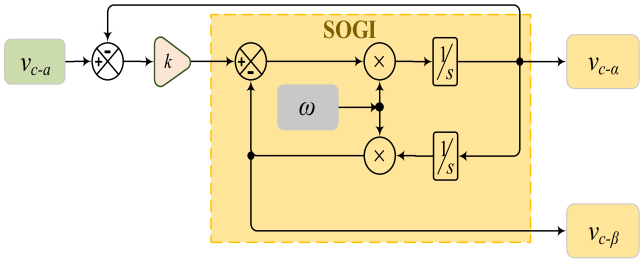

FIGURE 8 | Basic structure of SOGI-QSG.

as a second-order system, with the filtered signal and its quadrature counterpart generated by a gain parameter that controls response speed. The following differential equations can describe it:

$$\begin{cases} \dot{v}_{c-\alpha}(t) = k\omega[v_c(t) - v_\alpha(t)] - \omega v_\beta(t) \\ \dot{v}_{c-\beta}(t) = \omega v_\alpha(t) \end{cases} \tag{17}$$

In this setup, the SOGI functions as an adaptive resonant controller offering selective amplification at ω_0 while attenuating harmonics and noise components outside the bandwidth with a pair of complex-conjugate poles tuned to the fundamental frequency. Based on the internal model principle, integrating the SOGI into a unity feedback control loop (FLL or PLL) allows for the extraction of the fundamental component of a single-phase input signal, along with its quadrature (90° phase-shifted) counterpart. To ensure accurate frequency tracking, the frequency estimator dynamically adjusts the SOGI's center frequency. The differential equation governing this estimation process is derived using the gradient descent method, expressed as

$$\dot{\hat{\omega}} = -\gamma v_\alpha(t) v_\beta(t) \tag{18}$$

where $\hat{\omega}$ is the estimated frequency and γ is typically chosen between 0.1 and 1 to balance fast convergence and noise robustness. The adaptation gain γ adjusts the convergence speed of the frequency estimator. A large γ ($\gamma > 1$) results in faster convergence but increased noise amplification, while a small γ ($\gamma < 0.1$) results in robust estimation but poor dynamic response. To ensure stability, γ must satisfy:

$$0 < \gamma < \frac{2k}{\omega_n} \tag{19}$$

where ω_n is the nominal angular frequency. Considering MG operation at 50 Hz and $k \approx 1.4$, the upper bound is $\gamma < 0.089$. However, under VICL operation, the estimator receives filtered $\alpha\beta$ components, which allow relaxed upper bounds, as indicated in [74]. Therefore, $\gamma = 0.5$ was selected because it provides fast tracking during disturbances (DG plug-in/out, load steps), avoids excessive oscillations in the estimated frequency, and remains within the stable region, as validated by the small-signal model in simulation. This structure enables real-time tracking of frequency drifts, enhancing synchronization accuracy.

The parameters were tuned using a combined procedure:

1. Small-signal pole placement to ensure SOGI closed-loop poles satisfy:
   - $\Re\{p_i\} < -220$ rad/s
2. Frequency-response shaping, constraining:
   - -3 dB bandwidth $\approx$ 15–25 Hz around the fundamental,
   - attenuation > 25 dB at 5th, 7th, and 11th harmonics.
3. Transient-performance constraints:
   - rise time < 10 ms,
   - overshoot < 10%,
   - phase-tracking error < 2° at steady state.
4. Validation through nonlinear, unbalanced, and harmonic-rich conditions, ensuring robustness across all operating scenarios.

During operation, frequency estimation is considered converged when:

$$|\dot{\hat{\omega}}(t)| < 0.1 \text{ rad/s}, \ |v_\alpha^2 + v_\beta^2 - \hat{A}^2| < 1\% \tag{20}$$

In simulations, convergence was consistently achieved within 2–3 grid cycles under nominal conditions and within five cycles during nonlinear or unbalanced operation.

SOGI offers key advantages, including effective harmonic filtering, fast dynamic response, and simple real-time implementation, making it useful in grid synchronization, power quality analysis, renewable energy integration, and fault detection. However, its basic form remains sensitive to harmonics, lacks automatic frequency adaptation, and struggles with sudden frequency variations.

To address these issues, several ESOGI variants have been proposed. ESOGI introduces a dynamic tuning mechanism to improve rejection of grid disturbances and reduce estimation delay [75]. The modified SOGI (MSOGI) structure supports multifrequency component tracking and is particularly suitable for power-sharing applications in MGs [36]. The dual SOGI (DSOGI) configuration extends the basic SOGI to enable simultaneous extraction of $\alpha\beta$ orthogonal components in both positive and negative sequences, proving effective under unbalanced conditions [76]. Other advanced configurations, such as n-SOGI, allow simultaneous estimation of multiple harmonics, making them suitable for active filtering and harmonic compensation.

These developments have significantly improved the applicability of SOGI-based methods in modern power systems, especially in MGs, where harmonic distortion, unbalanced loading, and dynamic conditions demand high-performance signal-processing strategies.

2.3.2 | ESOGI

The schematic of the designed VI intended for a three-phase VSI is depicted in Figure 9. As shown, the ESOGI uses the output current of the *a*-phase ($i_{L2.a\text{-}in}$), obtained via the *abc*-$\alpha\beta$ transform, to extract the filtered direct and orthogonal fundamental components ($i_{L2.\alpha\beta}$). Note that the ESOGI uses the frequency provided by the droop control. The $\alpha\beta$ components are multiplied by the virtual inductance, L_v, and the fundamental frequency, ω. The resulting $\alpha\beta$ voltage components are transformed to *abc* voltages. These *abc* voltages are, then, added to the terms obtained from the multiplication of *abc* components ($i_{L2.abc}$) with the virtual resistance, r_v, to obtain the output *abc* voltages of the VI.

Accordingly, the output of the VI, in the *s*-domain, can be derived as follows:

$$v_{z-abc}(s) = r_v i_{L2.abc} - \left(T_{\alpha\beta-abc} \times \left(L_v \omega \times \begin{bmatrix} -i_{L2.\beta} & i_{L2.\alpha} \end{bmatrix}^T\right)\right) \tag{21}$$

where $T_{\alpha\beta\text{-}abc}$ defines the inverse Clarke transform.

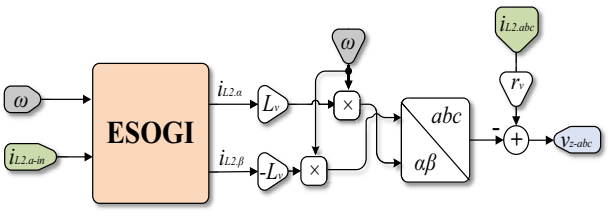

FIGURE 9 | Structure of the VI control scheme based on ESOGI.

The $\alpha\beta$ voltage components are transferred to abc frame and then subtracted from the ones generated by the droop controllers, resulting in the new voltage reference defined as follows:

$$v_{C\text{-ref}}(s) = v_{\text{droop-ref}}(s) - v_z(s) \tag{22}$$

The structure of the ESOGI used to estimate the current components is presented in Figure 10. It consists of two second-order adaptive filters, tuned by the droop control frequency and an LPF. The adaptive filters generate the $\alpha\beta$ current components from a single sinusoidal current, while the LPF oversees estimating the inherent DC offset in the input current. The outputs of the ESOGI are the direct component and the quadrature component free from the DC offset, which is achieved by subtracting the estimated DC offset from the shifted quadrature generated by the SOGI [11].

The ESOGI can accurately estimate the current components, even under distorted currents and fast dynamic responses, in addition to its simple implementation. This may improve droop control performance, thereby increasing power-sharing accuracy.

2.3.3 | MSOGI

The structure of the MSOGI used to estimate the current components is presented in Figure 11. It consists of four SOGI, each associated in parallel, corresponding to the fundamental, 5th, 7th, and 11th harmonic current estimations. The input of an SOGI corresponding to h harmonic ($h = 1; 5; 7; 11$) is the sum of all the other current components estimated by the other SOGIs, subtracted from the actual current. In addition, each SOGI is tuned to a frequency equal to the product of the droop control frequency and the respective h harmonic. An application of this scheme can be found in [33, 39]. The structure of the SOGI is shown in Figure 10, which accepts a sinusoidal single-voltage input and provides in-phase and quadrature-phase components as outputs. The harmonic components tracked by the MSOGI are subsequently utilized within the VICL to enhance harmonic compensation. Once the MSOGI isolates the dominant harmonics in the $\alpha\beta$ frame, these signals are used to synthesize compensating voltage references that are injected through the VI path. This process effectively counteracts voltage distortion at the PCC and enforces proportional harmonic current sharing among the distributed generators. Consequently, the MSOGI not only detects harmonic content but also contributes actively to improving overall power quality and maintaining balanced operation under nonlinear load conditions.

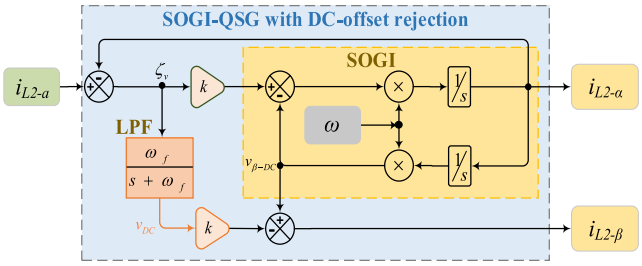

FIGURE 10 | ESOGI structure.

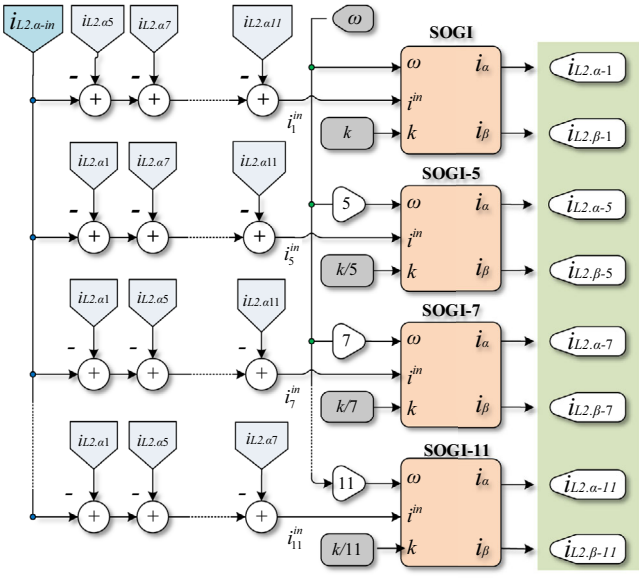

FIGURE 11 | Multiple-SOGI structure.

As a result, the MSOGI can estimate the current components with high accuracy, even under harmonically distorted current conditions, while providing a fast dynamic response. This may improve droop control performance, thereby increasing power-sharing accuracy.

2.3.4 | Dual Enhanced SOGI

The dual enhanced SOGI (DESOGI) technique, which introduces an additional loop for the estimation/rejection of the DC component, is an adaptive second-order filter used to estimate the essential characteristics of a three-phase input voltage [39]. Figure 12 shows the block diagram of the DESOGI structure. It is composed of two ESOGI-based QSG (ESOGI-QSG). The primary function of the ESOGI-QSG block is to extract the direct and orthogonal voltage components, which can be utilized to determine the voltage amplitude. The operational frequency supplied to the ESOGI-QSG blocks is estimated by FLL. Further details regarding this plan can be found in [39].

The relationship between the input MG voltage and the extracted orthogonal components ($\hat{v}_{\text{MG}_\alpha}, \hat{v}_{\text{MG}_\beta}$) can be described by the following closed-loop transfer functions [77], as shown in Figure 12:

$$\begin{cases} G_\alpha(s) = \dfrac{\hat{v}_{\text{MG}_\alpha}(s)}{v_{\text{MG}}(s)} = k\hat{\omega}_{\text{MG}} \dfrac{s}{s^2 + k\hat{\omega}_{\text{MG}} s + \hat{\omega}^2_{\text{MG}}} \\ G_\beta(s) = \dfrac{\hat{v}_{\text{MG}_\beta}(s)}{v_{\text{MG}}(s)} = \dfrac{k(\hat{\omega}^2_{\text{MG}} - \omega_{\text{f}} s)}{s + \omega_{\text{f}}} \dfrac{s}{s^2 + k\hat{\omega}_{\text{MG}} s + \hat{\omega}^2_{\text{MG}}} \\ G_{\beta-\text{DC}}(s) = \dfrac{\hat{v}_{\text{MG}_{\beta-DC}}(s)}{v_{\text{MG}}(s)} = \dfrac{k\hat{\omega}^2_{\text{MG}}}{s^2 + k\hat{\omega}_{\text{MG}} s + \hat{\omega}^2_{\text{MG}}} \end{cases} \tag{23}$$

In this equation, s represents the Laplace variable, $\hat{\omega}_{\text{MG}}$ and ω_{f} denote the estimated and the additional block frequencies, while k denotes the gain of the SOGI-QSG.

Similar to the other SOGI variants, the DESOGI operates in conjunction with an FLL that continuously tracks the fundamental frequency and adjusts the VICL's internal parameters in real time. This combined DESOGI-FLL structure provides accurate in-phase and quadrature components in the $\alpha\beta$ reference frame, enabling precise generation of compensating voltage references. Consequently, the VICL achieves improved synchronization, enhanced dynamic response, and superior harmonic and power-sharing performance among distributed generators.

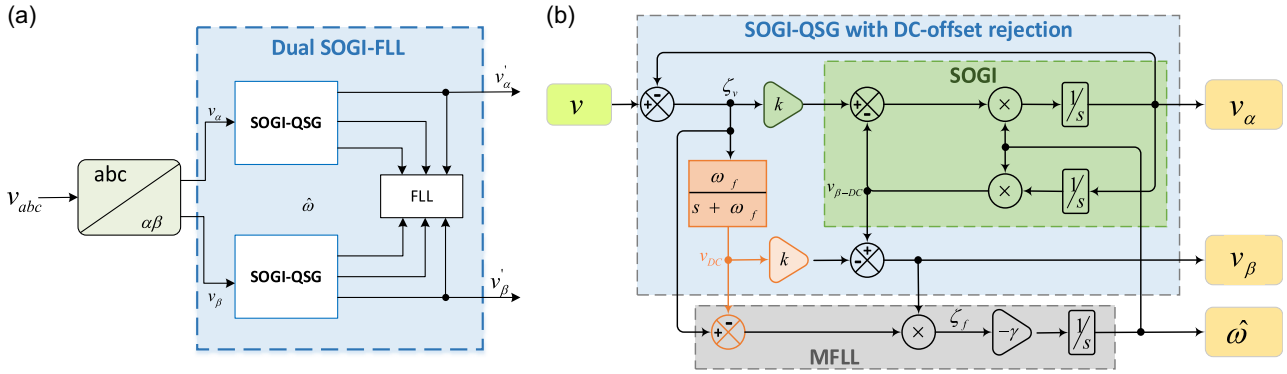

FIGURE 12 | The structure of (a) DESOGI-FLL and (b) ESOGI-FLL.

Authors in [78] provided additional information through theoretical analysis and a MATLAB/Simulink simulation study to confirm the accuracy of the generated frequency and amplitude models.

3 | Results and Discussion

To assess the effectiveness of the different control schemes, an MG model consisting of three inverters connected in parallel, feeding a common load, as shown in Figure 13, is built in MATLAB/Simulink. The controller under study is configured according to the parameters presented in Table 1. In this simulation, the performance of the designed controller is tested under various cases.

To ensure a fair comparative analysis, all SOGI-based controllers were tuned using the same search range, balancing time response and filtering performance. However, droop coefficients and filter parameters were selected based on standard design constraints ($\Delta f = 0.5$ Hz, $\Delta V = 5$ V).

While the DC/AC scaling was chosen for practical and design reasons ensuring an adequate modulation index and voltage margin for realistic inverter operation, following the typical IEC/EN LV standards: 220 Vrms (nominal low-voltage grid level in our region/230 V class per IEC/EN) represents a typical LV bus for residential/small MGs, and 450 Vdc was selected to provide sufficient headroom for the inverter modulation index and harmonic compensation.

3.1 | Test 01: Linear Load Changes

In this test, the dynamic performance of the DG units under linear load variations is evaluated. The DG units start with no load operation, with the first linear load being connected at $t = 0.05$ s.

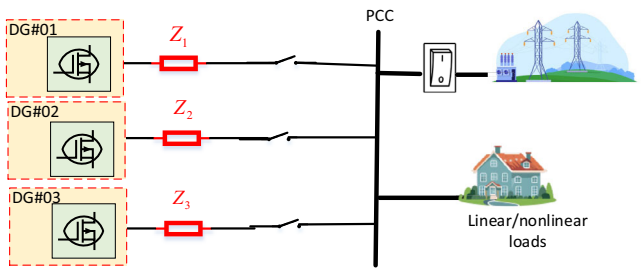

FIGURE 13 | Single-line diagram showing DG#1–DG#3 connections, PCC, load, and impedance.

TABLE 1 | VSIs and control parameter.

Parameters	Symbol	Unit	Value
Nominal voltage (RMS)	E_n	V	220
Nominal frequency	f_n	Hz	50
Switching frequency	f_s	kHz	20
Simulation frequency	f_e	MHz	1
DC voltage	U_{DC}	V	450
Output filter capacitor	C	μF	23
Output filter inductor	L,r	mH, Ω	2, 1
Line impedance of DG #1	L_1	mH, Ω	1.5, 0.8
Line impedance of DG #2	L_2	mH, Ω	0.5, 0.8
Line impedance of DG #3	L_3	mH, Ω	0.2, 0.8
Virtual inductance	L_v ,R_v	mH, Ω	2.7, 1
P–ω droop	m	rad/(W s)	0.0005
Q–V droop	n	V/Var	0.001
Voltage controller P gain	k_{pv}	—	0.1839
Voltage controller I gain	k_{pi}	—	183.87
Current controller P gain	k_{iv}	—	6.2831
Cutoff frequency	$f_{cut\text{-}off}$	kHz	1.5
SOGI parameters	k, γ	—	1.4, 0.5

Next, a second load is connected and disconnected at $t = 0.2$ and 0.5 s, respectively.

3.2 | Test 02: Nonlinear Load Changes

This second test evaluates the behavior of the proposed controllers under nonlinear load conditions. Similar to the previous test, the DG units are subjected to load variations, but in this case, the loads consist of rectifier bridges that introduce significant harmonic distortion into the system.

3.3 | Test 03: DG Units Plug In/Out

In this final test, the robustness of the proposed control strategies is evaluated during the connection and disconnection of DG units. Initially, only DG #1 supplies the load starting from $t = 0.1$ s. DG

TABLE 2 | Simulation results for SOGI method.

	SOGI method
TEST 01	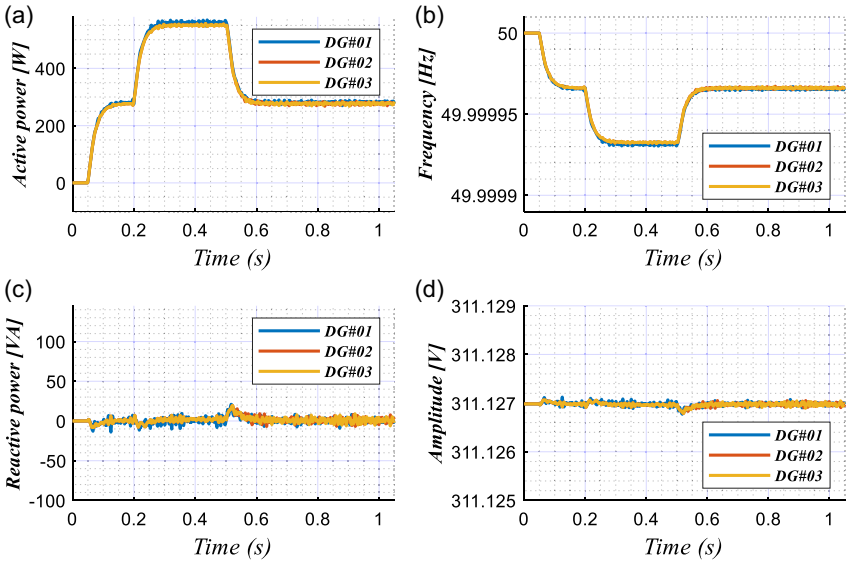
TEST 02	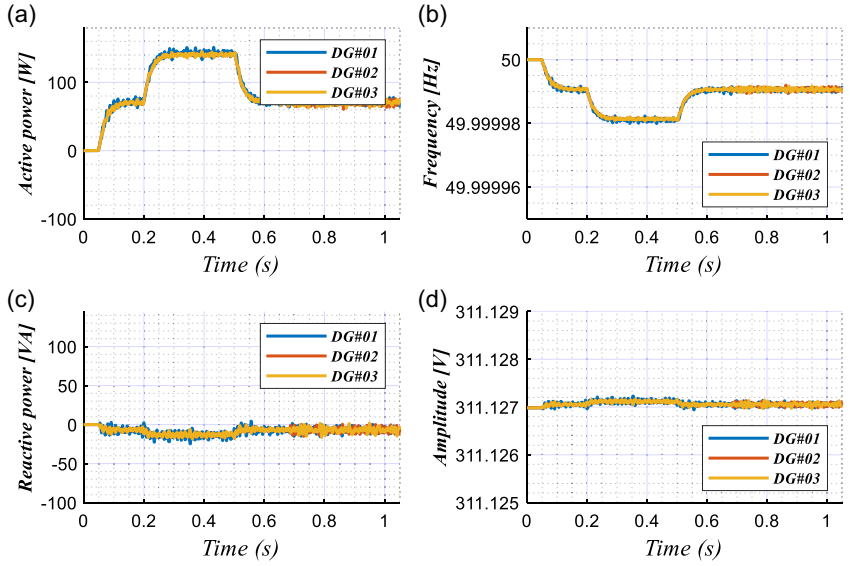
TEST 03	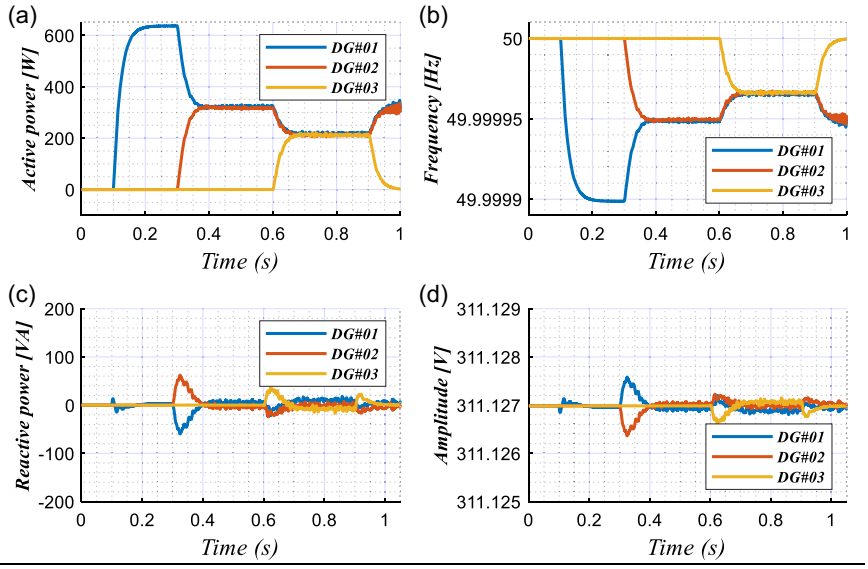

TABLE 3 | Simulation results for ESOGI method.

	ESOGI method
TEST 01	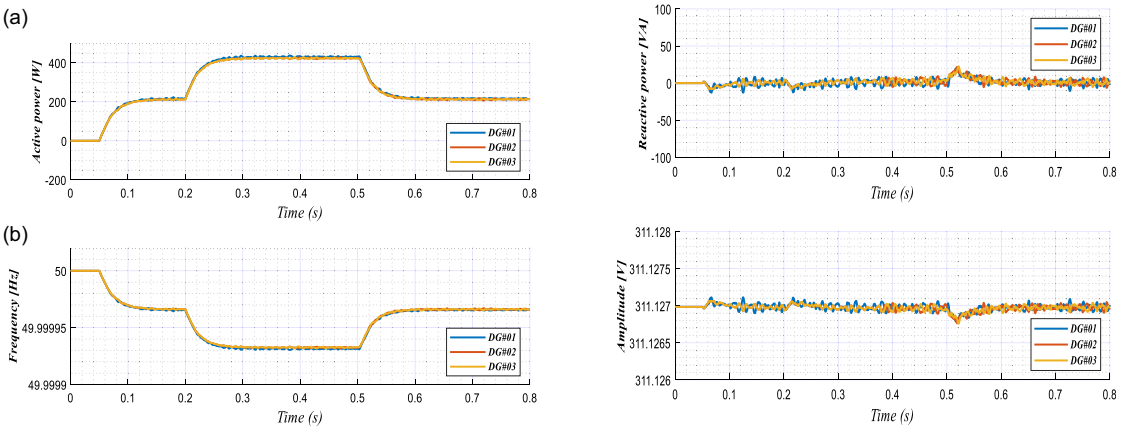
TEST 02	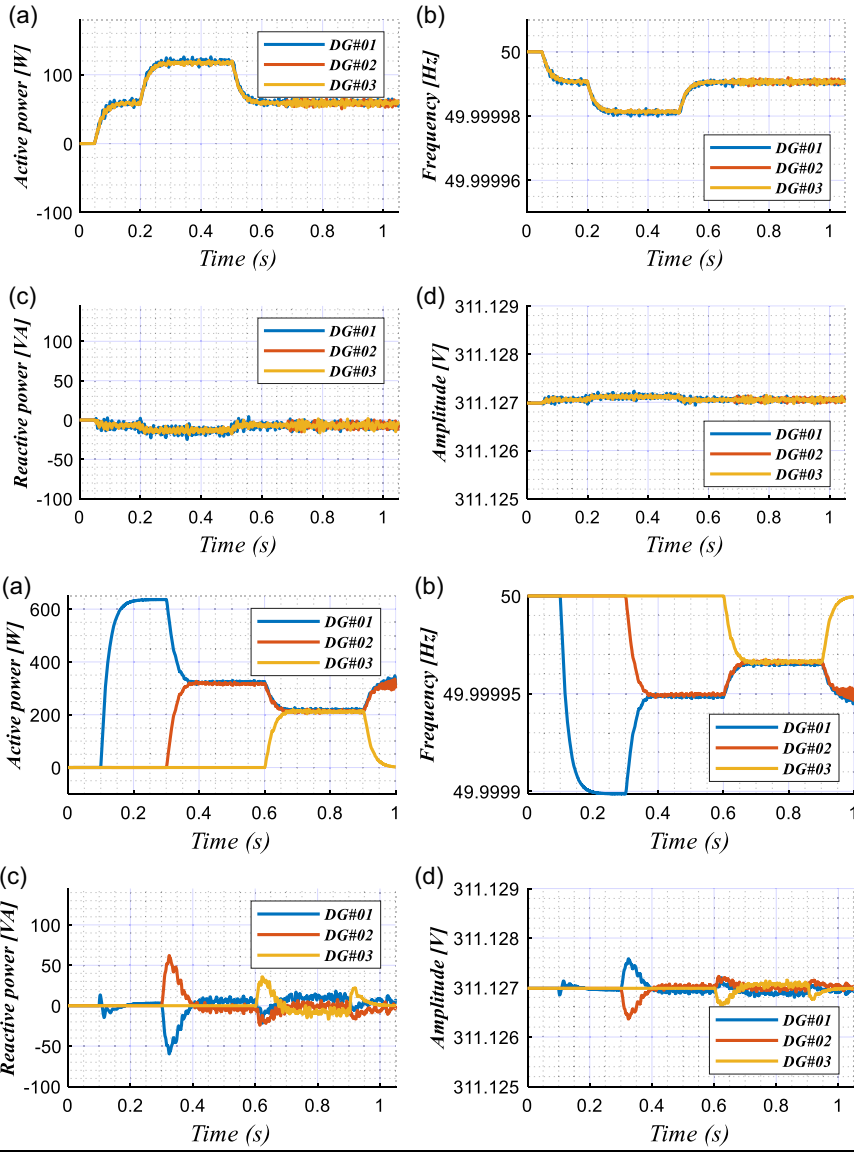
TEST 03	

#2 and DG #3 are then connected at $t = 0.3$s and $t = 0.6$ s, respectively, followed by the disconnection of DG #3 at $t = 0.9$ s.

Tables 2–5 illustrate the system's dynamic response, consistent with the previous test cases, for each SOGI variant method.

The simulation results obtained from the three test cases provide valuable insight into the performance of the proposed VI control schemes based on various SOGI variants. Across all tests, it is evident that the core objective—ensuring reliable power sharing

TABLE 4 | Simulation results for MSOGI method.

	MSOGI Method
TEST 01	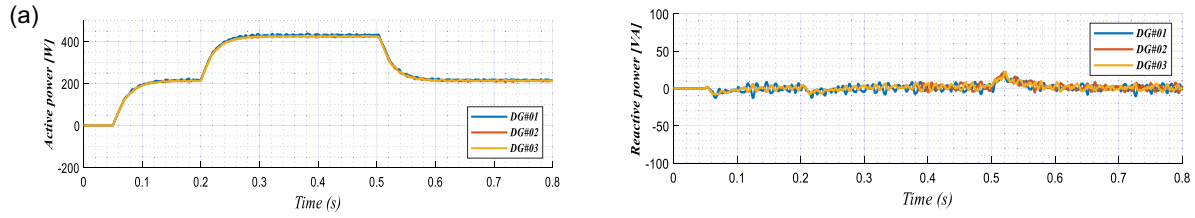
TEST 02	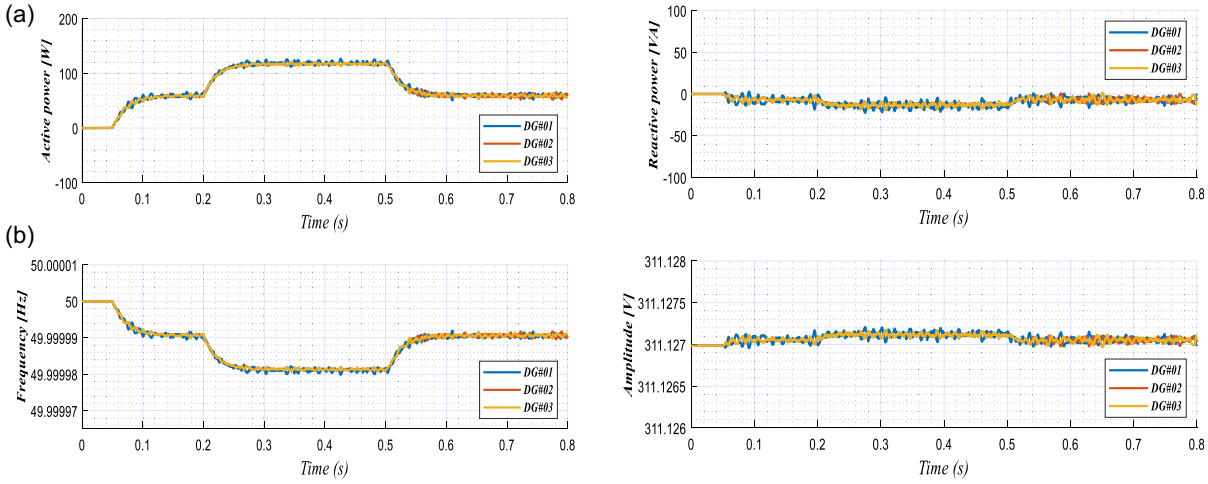
TEST 03	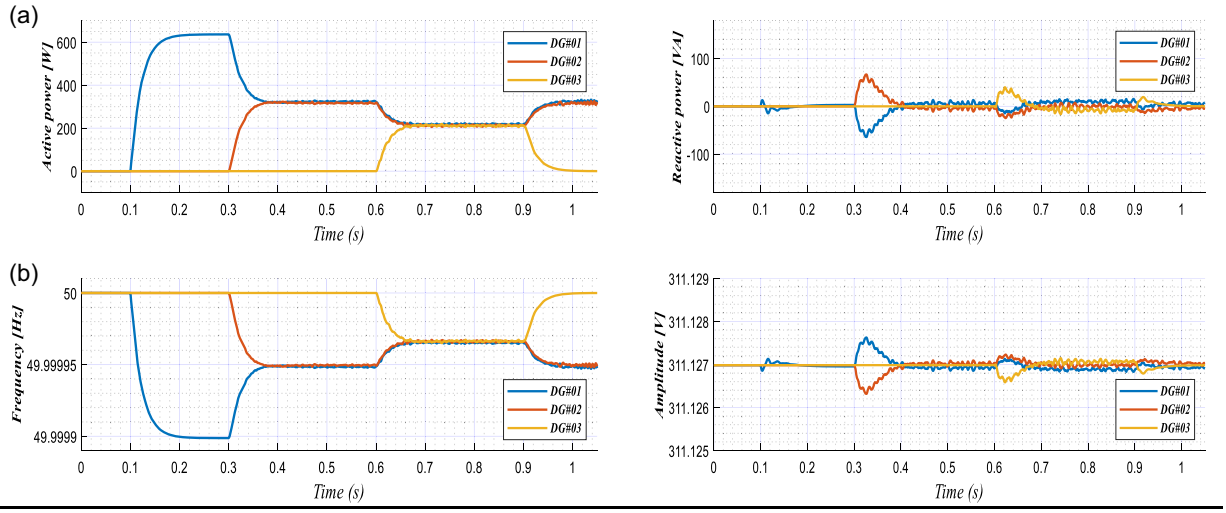

among DGs—is consistently achieved by each method under study. However, more nuanced differences emerge when examining the systems' dynamic response, harmonic handling, and robustness to configuration changes.

In the first test involving linear load variations, all controllers demonstrated effective active power sharing at steady state. This confirms the baseline capability of the VI structure to enforce proportional load distribution among DG units. Yet during transient periods, such as load connection or disconnection, notable disparities emerged. ESOGI and MSOGI, in particular, maintained smoother frequency responses with quicker recovery to nominal values. These improvements can be attributed to their adaptive tuning mechanisms, which enhance their ability to respond to fast-changing system dynamics.

The second test, which introduced nonlinear loads, further highlighted the advantages of using advanced SOGI structures. Despite the increased harmonic content and waveform distortion introduced by the rectifier-type loads, all controllers maintained

TABLE 5 | Simulation results for DSOGI method.

	DSOGI method
TEST 01	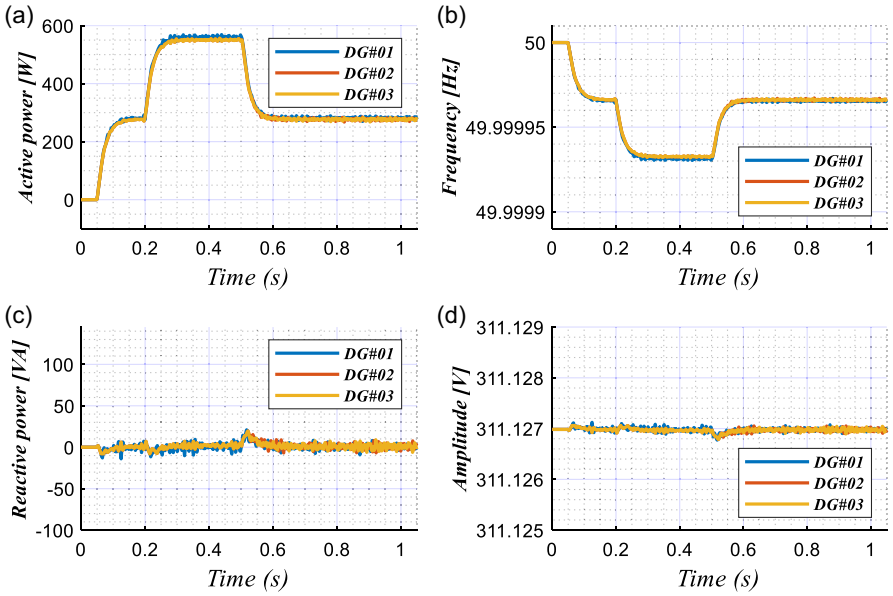
TEST **02**	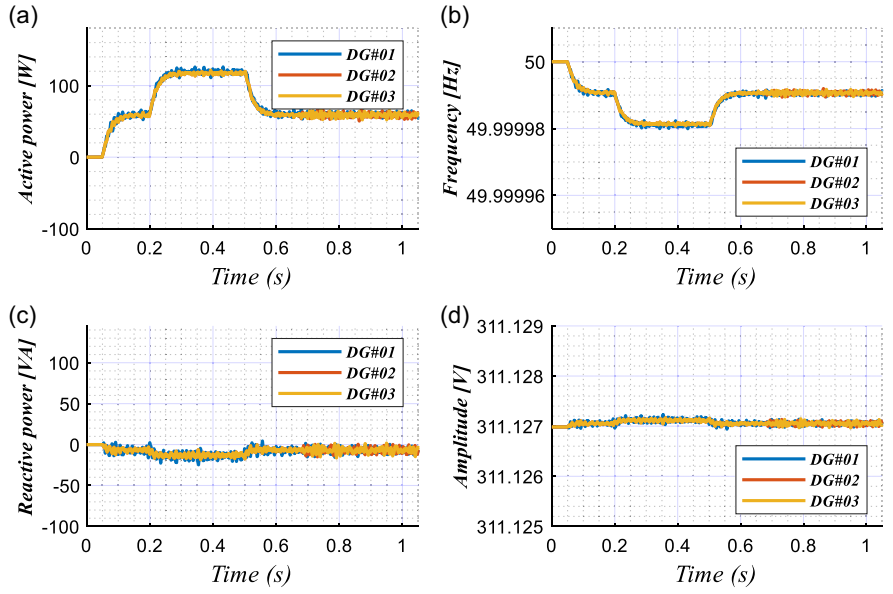
TEST **03**	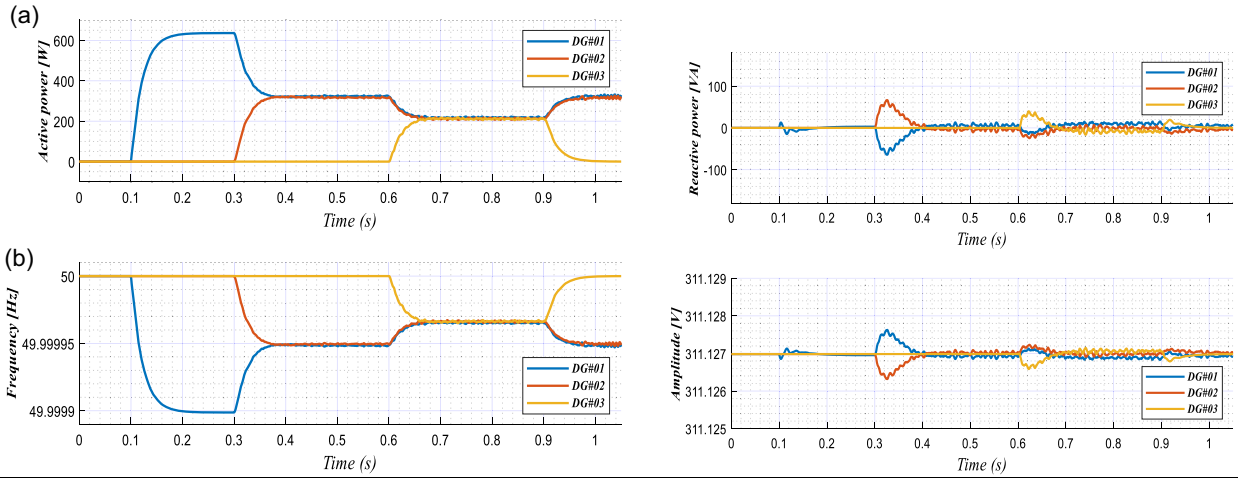

system stability and appropriate power sharing. Nonetheless, MSOGI and DSOGI clearly outperformed the others in terms of harmonic rejection and waveform quality. Their respective architectures—multifrequency tracking in MSOGI and dual-sequence filtering in DSOGI—proved highly effective in minimizing THD and preserving voltage quality at the PCC.

These traits make them especially well suited for MGs operating in environments with significant power electronics interference or nonlinear demand.

The third test evaluated the robustness of each controller during the plug-in and plug-out of DG units. While all methods continued to share active and reactive power effectively, the stability and smoothness of the transition varied. MSOGI and DSOGI once again demonstrated superior performance, maintaining voltage and frequency within close bounds of their nominal values and exhibiting minimal overshoot or oscillations. In contrast, the basic SOGI structure showed notable deviations during these transitions, indicating its limitations in handling dynamic reconfiguration events typical in real-world MGs.

Taken together, these findings suggest that while classical SOGI-based control schemes may suffice for steady-state conditions or low-disturbance environments, more advanced variants such as MSOGI and DSOGI offer tangible benefits in terms of dynamic performance, harmonic resilience, and system adaptability. These methods are therefore recommended for deployment in modern, flexible MGs where load variability, harmonic pollution, and plug-and-play functionality are expected.

The detailed quantitative results of each test case are summarized in Tables 2–5.

Table 6 shows that the simulation results clearly demonstrate how the various SOGI-based techniques affect MG power-sharing performance. As anticipated, the basic SOGI produces the poorest results, with considerable power-sharing mistakes, particularly in reactive power (over 10%), and high total harmonic distortion (5.2%). This is primarily because of its limited capacity to handle imbalanced and nonlinear conditions or to adapt to grid disruptions.

In contrast, ESOGI offers observable enhancements. It reduces THD and improves the accuracy of both active and reactive power sharing through its enhanced filtering and dynamic tuning. However, the performance truly shines with MSOGI and particularly DSOGI. While DSOGI performs best across all categories, including very low THD (1.9%), minimum power-sharing error

TABLE 6 | Performance comparison.

Method	SOGI	ESOGI	MSOGI	DESOGI
Injected current THD, %	5.2	3.6	2.1	1.9
Active power-sharing error, %	7.8	3.2	1.5	1.2
Reactive power-sharing error, %	10.4	4.5	2.3	1.8
Settling time, ms	45	35	28	26
Execution time, ms	0.93	1.09	1.27	1.84
Relative stability	Medium	High	Very high	Very high
Relative harmonic resistance	Low	Medium	Very high	High
Relative accuracy	Basic	Improved	High	Very high
Relative convergence speed	Fast	Fast	Medium	Fast
Relative complexity	Low	Moderate	High	Moderate

TABLE 7 | Main findings.

Method	DG plug-in/out	Sudden load variation	Nonlinear load feeding
SOGI (classic)	Struggles with transient oscillations when a DG unit is added/removed. Frequency deviations are noticeable.	Responds slowly to sudden load changes, leading to temporary power-sharing imbalances.	Sensitive to harmonics, causing inaccurate frequency estimation and distorted voltage waveforms.
ESOGI	Better than classic SOGI in handling transients. It dynamically adapts to limit frequency deviations, but still faces challenges in fast-changing conditions.	Improved response to load variations by dynamically adjusting gain, but still susceptible to overshoot.	Moderately robust in nonlinear load conditions, but can still experience phase errors.
DSOGI	Designed for three-phase systems, ensures smooth DG integration and minimizes unbalanced currents when the DG is plugged in/out.	More stable than SOGI/ESOGI as it separates positive and negative sequences, reducing transient oscillations.	Performs well under unbalanced nonlinear loads, effectively filtering out negative-sequence harmonics.
MSOGI	The most robust against DG plug-in/out effects. It ensures minimal transient oscillations and faster stabilization.	Highly responsive to sudden load changes, keeping power-sharing accurate and stable.	Excels in harmonic rejection, making it ideal for nonlinear loads with high distortion

(about 1% to 2%), and a quick dynamic response with a settling time of just 26 ms, MSOGI performs well under harmonic distortion.

These findings demonstrate that more sophisticated structures, especially DSOGI, are better suited to demanding MG settings with frequent harmonics, load imbalances, and dynamic fluctuations. Nevertheless, since more sophisticated filters like DSOGI require more processing and tuning, the technique selection should still consider implementation complexity and real-time constraints. Each SOGI variant offers a distinct trade-off: SOGI provides simplicity; ESOGI improves DC offset rejection; MSOGI provides balanced accuracy and speed; and DSOGI achieves the best accuracy at a higher computational cost. So, the established performance hierarchy, DSOGI > MSOGI > ESOGI > SOGI, emphasizes the intrinsic trade-off between estimation accuracy and computational complexity, indicating that higher precision and harmonic compensation capability are achieved at the expense of increased processing effort.

Note that the proposed approach scales efficiently for larger MGs with more than three DG units, though communication latency and line impedance diversity may affect performance.

Meanwhile, Table 7 highlights the study's key findings through a comparative examination of the approaches considered for VI application in MGs.

4 | Conclusions

In this article, a power-sharing control with a VICL based on different SOGI variants was presented for an islanded MG. The study developed the theoretical foundation for droop-controller VSIs, described the structure of the proposed VICL, and provided the corresponding mathematical formulation. In addition, it provided a detailed analysis of four SOGI variants—SOGI, ESOGI, MSOGI, and DESOGI—in terms of power sharing, harmonic mitigation, and dynamic performance. A simulation model of a three-DG MG was conducted in MATLAB/Simulink to assess and validate the proposed controller.

The results obtained highlight the strengths and limitations of different SOGI variants in MG applications. The classic SOGI is effective in simple, minimally disturbed systems. It performs effectively under ideal conditions; however, its performance remains limited in the presence of disturbances. In contrast, ESOGI enhances DC-offset rejection, improving both robustness and frequency stability, making it more resilient in complex environments. Meanwhile, MSOGI proves highly effective in environments with significant harmonic distortion, offering superior performance in mitigating these disturbances. Likewise, DSOGI is particularly well suited for three-phase MGs with imbalances, as it is specifically designed to handle such challenges effectively. Quantitatively, the DSOGI-based VICL reduced THD from 5.2% to 1.9% and decreased power-sharing error from 7.8% to 1.2%, confirming significant performance improvements over the classical SOGI scheme.

In practice, computational demand increases with higher order SOGI structures, especially for DSOGI. Nevertheless, the proposed VICL framework remains scalable for systems with more than three distributed generators using decentralized, communication-free control. These findings provide valuable insights into the design of accurate and adaptive controllers for future MG applications.

Future work will focus on experimental validation through small-scale hardware prototypes and hardware-in-the-loop testing to confirm the real-time feasibility of the proposed control strategy. Moreover, reinforcement learning-based adaptive SOGI tuning and integration with advanced phase-locked loop techniques will be explored to further enhance adaptability and real-world performance.

Funding

The authors have nothing to report.

Data Availability Statement

The data that support the findings of this study are available from the corresponding author upon reasonable request.

References

1. J. M. Guerrero, L. Garcia de Vicuna, J. Matas, M. Castilla, and J. Miret, "Output Impedance Design of Parallel-Connected UPS Inverters with Wireless Load-Sharing Control," *IEEE Transactions on Industrial Electronics* 52, no. 4 (2005): 1126–1135, https://doi.org/10.1109/TIE.2005.851634.

2. N. Nasser and M. Fazeli, "Buffered-Microgrid Structure for Future Power Networks; a Seamless Microgrid Control," *IEEE Transactions on Smart Grid* 12, no. 1 (2021): 131–140, https://doi.org/10.1109/TSG.2020.3015573.

3. J. M. Guerrero, J. C. Vasquez, J. Matas, L. G. d. Vicuna, and M. Castilla, "Hierarchical Control of Droop-Controlled AC and DC Microgrids—A General Approach Toward Standardization," *IEEE Transactions on Industrial Electronics* 58, no. 1 (2011): 158–172, https://doi.org/10.1109/TIE.2010.2066534.

4. E. Kabalcı, "Hierarchical Control in Microgrid," in *Microgrid Architectures, Control and Protection Methods. Power Systems*, ed. N. Mahdavi Tabatabaei, E. Kabalci, and N. Bizon (Springer, 2019), 381–401, https://doi.org/10.1007/978-3-030-23723-3_15.

5. B. Keyvani-Boroujeni, B. Fani, G. Shahgholian, and H. H. Alhelou, "Virtual Impedance-Based Droop Control Scheme to Avoid Power Quality and Stability Problems in VSI-Dominated Microgrids," *IEEE Access* 9 (2021): 144999–145011, https://doi.org/10.1109/ACCESS.2021.3122800.

6. B. M. Eid, N. A. Rahim, J. Selvaraj, and A. Elkhateb, "Control Methods and Objectives for Electronically Coupled Distributed Energy Resources in Microgrids: A Review," *IEEE Systems Journal* 10, no. 2 (2016): 446–458, https://doi.org/10.1109/JSYST.2013.2296075.

7. W. R. Issa, A. Elkhateb, M. A. Abusara, and T. K. Mallick, "Control Strategy for Uninterrupted Microgrid Mode Transfer During Unintentional Islanding Scenarios," *IEEE Transactions on Industrial Electronics* 65, no. 6 (2018): 4831–4839, https://doi.org/10.1109/TIE.2017.2772199.

8. R. R. Kolluri, I. Mareels, T. Alpcan, M. Brazil, J. de Hoog, and D. A. Thomas, "Power Sharing in Angle Droop Controlled Microgrids," *IEEE Transactions on Power Systems* 32, no. 6 (2017): 4743–4751, https://doi.org/10.1109/TPWRS.2017.2672569.

9. A. Tah and D. Das, "An Enhanced Droop Control Method for Accurate Load Sharing and Voltage Improvement of Isolated and Interconnected DC Microgrids," *IEEE Transactions on Sustainable Energy* 7, no. 3 (2016): 1194–1204, https://doi.org/10.1109/TSTE.2016.2535264.

10. W. Issa, A. El Khateb, N. Anani, and M. Abusara, "Smooth Mode Transfer in AC Microgrids during Unintentional Islanding," *Energy Procedia* 134 (2017): 12–20, https://doi.org/10.1016/j.egypro.2017.09.592.

11. L. Zheng, C. Zhuang, J. Zhang, and X. Du, "An Enhanced Droop Control Scheme for Islanded Microgrids," *International Journal of Control and Automation* 8, no. 4 (2015): 63–74, https://doi.org/10.14257/ijca.2015.8.4.08.

12. E. Buraimoh and I. E. Davidson, "Fault Ride-Through Analysis of Current- and Voltage-Source Models of Grid Supporting Inverter-Based Microgrid," *IEEE Canadian Journal of Electrical and Computer Engineering* 44, no. 2 (2021): 189–198, https://doi.org/10.1109/ICJECE.2020.3035036.

13. X. Liang, C. Andalib-Bin-Karim, W. Li, M. Mitolo, and M. N. S. K. Shabbir, "Adaptive Virtual Impedance-Based Reactive Power Sharing in Virtual Synchronous Generator Controlled Microgrids," *IEEE Transactions on Industry Applications* 57, no. 1 (2021): 46–60, https://doi.org/10.1109/TIA.2020.3039223.

14. F. Göthner, J. Roldán-Pérez, R. E. Torres-Olguin, and O. M. Midtgård, "Harmonic Virtual Impedance Design for Optimal Management of Power Quality in Microgrids," *IEEE Transactions on Power Electronics* 36, no. 9 (2021): 10114–10126, https://doi.org/10.1109/TPEL.2021.3065755.

15. Z. Jin and X. Wang, "A DQ-Frame Asymmetrical Virtual Impedance Control for Enhancing Transient Stability of Grid-Forming Inverters," *IEEE Transactions on Power Electronics* 37, no. 4 (2022): 4535–4544, https://doi.org/10.1109/TPEL.2021.3124286.

16. R. An, Z. Liu, and J. Liu, "Successive-Approximation-Based Virtual Impedance Tuning Method for Accurate Reactive Power Sharing in Islanded Microgrids," *IEEE Transactions on Power Electronics* 36, no. 1 (2021): 87–102, https://doi.org/10.1109/TPEL.2020.3001037.

17. J. He and Y. W. Li, "Analysis, Design, and Implementation of Virtual Impedance for Power Electronics Interfaced Distributed Generation," *IEEE Transactions on Industry Applications* 47, no. 6 (2011): 2525–2538, https://doi.org/10.1109/TIA.2011.2168592.

18. J. M. Guerrero, J. Matas, L. G. D. V. D. Vicuna, M. Castilla, and J. Miret, "Wireless-Control Strategy for Parallel Operation of Distributed-Generation Inverters," *IEEE Transactions on Industrial Electronics* 53, no. 5 (2006): 1461–1470, https://doi.org/10.1109/TIE.2006.882015.

19. J. He, L. Du, B. Liang, Y. Li, and C. Wang, "A Coupled Virtual Impedance for Parallel AC/DC Converter Based Power Electronics System," *IEEE Transactions on Smart Grid* 10, no. 3 (2019): 3387–3400, https://doi.org/10.1109/TSG.2018.2825383.

20. L. Lin, H. Ma, and Z. Bai, "An Improved Proportional Load-Sharing Strategy for Meshed Parallel Inverters System With Complex Impedances," *IEEE Transactions on Power Electronics* 32, no. 9 (2017): 7338–7351, https://doi.org/10.1109/TPEL.2016.2630709.

21. H. Mahmood, D. Michaelson, and J. Jiang, "Accurate Reactive Power Sharing in an Islanded Microgrid Using Adaptive Virtual Impedances," *IEEE Transactions on Power Electronics* 30, no. 3 (2015): 1605–1617, https://doi.org/10.1109/TPEL.2014.2314721.

22. H. Zhang, S. Kim, Q. Sun, and J. Zhou, "Notice of Removal: Distributed Adaptive Virtual Impedance Control for Accurate Reactive Power Sharing Based on Consensus Control in Microgrids," *IEEE Transactions on Smart Grid* 8, no. 4 (2017): 1749–1761, https://doi.org/10.1109/TSG.2015.2506760.

23. S. Chaturvedi, D. Fulwani, and J. M. Guerrero, "Adaptive-SMC Based Output Impedance Shaping in DC Microgrids Affected by Inverter Loads," *IEEE Transactions on Sustainable Energy* 11, no. 4 (2020): 2940–2949, https://doi.org/10.1109/TSTE.2020.2982414.

24. B. Wei, A. Marzàbal, R. Ruiz, J. M. Guerrero, and J. C. Vasquez, "DAVIC: A New Distributed Adaptive Virtual Impedance Control for Parallel-Connected Voltage Source Inverters in Modular UPS System," *IEEE Transactions on Power Electronics* 34, no. 6 (2019): 5953–5968, https://doi.org/10.1109/TPEL.2018.2869870.

25. T. V. Hoang and H. H. Lee, "Virtual Impedance Control Scheme to Compensate for Voltage Harmonics With Accurate Harmonic Power Sharing in Islanded Microgrids," *IEEE Journal of Emerging and Selected Topics in Power Electronics* 9, no. 2 (2021): 1682–1695, https://doi.org/10.1109/JESTPE.2020.2983447.

26. W. Feng, K. Sun, Y. Guan, J. M. Guerrero, and X. Xiao, "Active Power Quality Improvement Strategy for Grid-Connected Microgrid Based on Hierarchical Control," *IEEE Transactions on Smart Grid* 9, no. 4 (2018): 3486–3495, https://doi.org/10.1109/TSG.2016.2633298.

27. B. Ren, X. Sun, S. Chen, and H. Liu, "A Compensation Control Scheme of Voltage Unbalance Using a Combined Three-Phase Inverter in an Islanded Microgrid," *Energies* 11, no. 9 (2018): 2486, https://doi.org/10.3390/en11092486.

28. A. S. Vijay, S. Doolla, and M. C. Chandorkar, "Unbalance Mitigation Strategies in Microgrids," *IET Power Electronics* 13, no. 9 (2020): 1687–1710, https://doi.org/10.1049/iet-pel.2019.1080.

29. H. S. Ko, M. S. Jang, K. S. Ryu, D. J. Kim, and B. K. Kim, "Supervisory Power Quality Control Scheme for a Grid-Off Microgrid," *IEEE Transactions on Sustainable Energy* 9, no. 3 (2018): 1003–1010, https://doi.org/10.1109/TSTE.2017.2747591.

30. J. M. Alcala, M. Castilla, L. G. de Vicuña, J. Miret, and J. C. Vasquez, "Virtual Impedance Loop for Droop-Controlled Single-Phase Parallel Inverters Using a Second-Order General-Integrator Scheme," *IEEE Transactions on Power Electronics* 25, no. 12 (2010): 2993–3002, https://doi.org/10.1109/TPEL.2010.2082003.

31. X. Xiaofei, J. Yaoqin, H. Changhua, Y. Xumeng, W. Zechen, and G. Benhui, "An Enhanced Microgrid Power Sharing Strategy Based on Multiple Second Order Generalized Integrators Harmonic Detection and Adaptive Virtual Impedancee," in *2016 IEEE PES Asia-Pacific Power and Energy Engineering Conference (APPEEC)* (IEEE, 2016), 2343–2347, https://doi.org/10.1109/APPEEC.2016.7779903.

32. Y. Su, S. Liu, X. Zhao, and X. Chen, "An Improved Power Control with Virtual Impedance Based on a Second-Order General-Integrator," in *2015 34th Chinese Control Conference (CCC)* (IEEE, 2015), 9037–9042, https://doi.org/10.1109/ChiCC.2015.7261069.

33. C. A. Hammouda, R. Bradai, A. BendibA. Kherbachi, R. Boukenoui, and K. Kara, "ESOGI-Based Virtual Impedance Control Scheme with Performance Improvement for Droop-Operated Three-Phase VSIs in Islanded AC Microgrid," *paper presented at the 2023 International Conference on Renewable Solutions for Ecosystems: Towards a Sustainable Energy Transition ICRSEtoSET, DJELFA, Algeria*, 2023.

34. Z. Xin, R. Zhao, P. Mattavelli, P. C. Loh, and F. Blaabjerg, "Re-Investigation of Generalized Integrator Based Filters From a First-Order-System Perspective," *IEEE Access* 4 (2016): 7131–7144, https://doi.org/10.1109/ACCESS.2016.2616838.

35. X. Lin, R. Zamora, and C. Baguley, "Droop Control Based on Improved Virtual Impedance in a Stand-Alone Microgrid," *in 2019 IEEE PES GTD Grand International Conference and Exposition Asia (GTD Asia)* (IEEE, 2019), 883–888, https://doi.org/10.1109/GTDAsia.2019.8716027.

36. A. Kherbachi, A. Bendib, A. Chouder, H. Ahmed, M. Benbouzid, and S. Motahhir, "Design and Analysis of Virtual Impedance Control Scheme Based on MESOGI for Improving Harmonic Sharing of Nonlinear Loads," *Scientific Reports* 14, no. 1 (2024): 13356, https://doi.org/10.1038/s41598-024-62739-z.

37. M. Anwar, M. I. Marei, and A. A. El-Sattar, "Generalized Droop-Based Control for an Islanded Microgrid," *in 2017 12th International Conference on Computer Engineering and Systems (ICCES)* (IEEE, 2017), 717–722, https://doi.org/10.1109/ICCES.2017.8275399.

38. R. Moslemi and J. Mohammadpour, "Accurate Reactive Power Control of Autonomous Microgrids Using an Adaptive Virtual Inductance Loop," *Electric Power Systems Research* 129 (2015): 142–149, https://doi.org/10.1016/j.epsr.2015.08.001.

39. A. Kherbachi, A. Chouder, A. Bendib, K. Kara, and S. Barkat, "Enhanced Structure of Second-Order Generalized Integrator Frequency-Locked Loop Suitable for DC-Offset Rejection in Single-

Phase Systems," *Electric Power Systems Research, Elsevier,* 170 (2019): 348–357, https://doi.org/10.1016/j.epsr.2019.01.029.

40. V. Verma and G. G. Talpur, "Decentralized Master-Slave Operation of Microgrid Using Current Controlled Distributed Generation Sources," in *2012 IEEE International Conference on Power Electronics, Drives and Energy Systems (PEDES)* (IEEE, 2012), 1–6, https://doi.org/10.1109/PEDES.2012.6484502.

41. G. G. Talapur, H. M. Suryawanshi, A. B. Shitole, R. R. Deshmukh, and M. S. Ballal, "Master-Slave Control Based Reliable Micro-Grid with Back-to-Back Voltage Source Converter as Master DG," in *IECON 2017 – 43rd Annual Conference of the IEEE Industrial Electronics Society* (IIEEE, 2017), 310–315, https://doi.org/10.1109/IECON.2017.8216056.

42. L. K. Vedulla and M. K. Mishra, "*PSO Based Power Sharing Scheme for an Islanded DC Microgrid System," in IECON 2017 – 43rd Annual Conference of the IEEE Industrial Electronics Society* (2017), 392–397, https://doi.org/10.1109/IECON.2017.8216070.

43. J. M. Guerrero, M. Chandorkar, T. L. Lee, and P. C. Loh, "Advanced Control Architectures for Intelligent Microgrids—Part I: Decentralized and Hierarchical Control," *IEEE Transactions on Industrial Electronics* 60, no. 4 (2013): 1254–1262, https://doi.org/10.1109/TIE.2012.2194969.

44. A. Micallef, M. Apap, C. Spiteri-Staines, and J. M. Guerrero, "Single-Phase Microgrid With Seamless Transition Capabilities Between Modes of Operation," *IEEE Transactions on Smart Grid* 6, no. 6 (2015): 2736–2745, https://doi.org/10.1109/TSG.2015.2444912.

45. J. M. Guerrero, L. G. d. Vicuna, J. Matas, M. Castilla, and J. Miret, "A Wireless Controller to Enhance Dynamic Performance of Parallel Inverters in Distributed Generation Systems," *IEEE Transactions on Power Electronics*, 19, no. 5 (IEEE, 2004): 1205–1213, https://doi.org/10.1109/TPEL.2004.833451.

46. Z. Jiang and X. Yu, "Active Power—Voltage Control Scheme for Islanding Operation of Inverter-Interfaced Microgrids," in *2009 IEEE Power & Energy Society General Meeting* (IEEE, 2009), 1–7, https://doi.org/10.1109/PES.2009.5275754.

47. H. Ye, Y. Liu, W. Pei, and L. Kong, "Efficient Droop-Based Primary Frequency Control from Variable-Speed Wind Turbines and Energy Storage Systems," in *2017 IEEE Transportation Electrification Conference and Expo, Asia-Pacific (ITEC Asia-Pacific)* (IEEE, 2017), 1–5, https://doi.org/10.1109/ITEC-AP.2017.8080968.

48. A. Bendib, A. Kherbachi, K. Kara, and A. Chouder, "*Droop Controller Based Primary Control Scheme for Parallel-Connected Single-Phase Inverters in Islanded AC Microgrid," in 2017 5th International Conference on Electrical Engineering – Boumerdes (ICEE-B)* (2017), 1–6, https://doi.org/10.1109/ICEE-B.2017.8192019.

49. J. W. Simpson-Porco, F. Dörfler, and F. Bullo, "Synchronization and Power Sharing for Droop-Controlled Inverters in Islanded Microgrids," *Automatica* 49, no. 9 (2013): 2603–2611, https://doi.org/10.1016/j.automatica.2013.05.018.

50. H. Mahmood, D. Michaelson, and J. Jiang, "A Power Management Strategy for PV/Battery Hybrid Systems in Islanded Microgrids," *IEEE Journal of Emerging and Selected Topics in Power Electronics, IEEE,* 2, no. 4 (2014): 870–882, https://doi.org/10.1109/JESTPE.2014.2334051.

51. Y. Wang, H. Jiang, L. Zhou, and P. Xing, "*An Improved Adaptive Droop Control Strategy for Power Sharing in Micro-Grid," in 8th International Conference on Intelligent Human-Machine Systems and Cybernetics (IHMSC)* (2016), vol. 01, 50–53, https://doi.org/10.1109/IHMSC.2016.97.

52. A. Bidram and A. Davoudi, "Hierarchical Structure of Microgrids Control System," *IEEE Transactions on Smart Grid* 3, no. 4 (2012): 1963–1976, https://doi.org/10.1109/TSG.2012.2197425.

53. T. V. Vu, S. Paran, F. Diaz-Franco, T. El-Mezyani, and C. S. Edrington, "An Alternative Distributed Control Architecture for Improvement in the Transient Response of DC Microgrids," *IEEE Transactions on Industrial Electronics, IEEE,* 64, no. 1 (2017): 574–584, https://doi.org/10.1109/TIE.2016.2607681.

54. F. Alam, M. Ashfaq, S. S. Zaidi, and A. Y. Memon, "*Robust Droop Control Design for a Hybrid AC/DC Microgrid," in 2016 UKACC 11th International Conference on Control (CONTROL)* (2016), 1–6, https://doi.org/10.1109/CONTROL.2016.7737547.

55. S. Sinha, S. Ghosh, and P. Bajpai, "Power Sharing through Interlinking Converters in Adaptive Droop Controlled Multiple Microgrid System," *International Journal of Electrical Power & Energy Systems* 128 (2021): 106649, https://doi.org/10.1016/j.ijepes.2020.106649.

56. Y. Han, H. Li, P. Shen, E. A. A. Coelho, and J. M. Guerrero, "Review of Active and Reactive Power Sharing Strategies in Hierarchical Controlled Microgrids," *IEEE Transactions on Power Electronics* 32, no. 3 (2017): 2427–2451, https://doi.org/10.1109/TPEL.2016.2569597.

57. H. Han, Y. Liu, Y. Sun, M. Su, and J. M. Guerrero, "An Improved Droop Control Strategy for Reactive Power Sharing in Islanded Microgrid," *IEEE Transactions on Power Electronics* 30, no. 6 (2015): 3133–3141, https://doi.org/10.1109/TPEL.2014.2332181.

58. Y. Gupta, K. Chatterjee, and S. Doolla, "A Simple Control Scheme for Improving Reactive Power Sharing in Islanded Microgrid," *IEEE Transactions on Power Systems* 35, no. 4 (2020): 3158–3169, https://doi.org/10.1109/TPWRS.2020.2970476.

59. U. B. Tayab, M. A. B. Roslan, L. J. Hwai, and M. Kashif, "A Review of Droop Control Techniques for Microgrid," *Renewable and Sustainable Energy Reviews, Elsevier,* 76 (2017): 717–727, https://doi.org/10.1016/j.rser.2017.03.028.

60. L. Li, Y. Han, P. Yang, Q. Huang, Z. Zhang, and Y. Xu, *A New Distributed Control Strategy for DC Microgrids with Droop Coefficient Correction and DC Bus Voltage Restoration," in 2019 IEEE Innovative Smart Grid Technologies – Asia (ISGT Asia)* (2019), 3908–3913, https://doi.org/10.1109/ISGT-Asia.2019.8881782.

61. X. H. T. Pham, "Power Sharing Strategy in Islanded Microgrids Using Improved Droop Control," *Electric Power Systems Research, Elsevier,* 180 (2020): 106164, https://doi.org/10.1016/j.epsr.2019.106164.

62. R. Hidalgo-León, C. Sanchez-Zurita, P. Jácome-Ruiz, J. Wu, and Y. Muñoz-Jadan, "*Roles, Challenges, and Approaches of Droop Control Methods for Microgrids," in 2017 IEEE PES Innovative Smart Grid Technologies Conference – Latin America (ISGT Latin America)* (2017), 1–6, https://doi.org/10.1109/ISGT-LA.2017.8126695.

63. Z. Shuai, S. Mo, J. Wang, Z. J. Shen, W. Tian, and Y. Feng, "Droop Control Method for Load Share and Voltage Regulation in High-Voltage Microgrids," *Journal of Modern Power Systems and Clean Energy* 4, no. 1 (2016): 76–86, https://doi.org/10.1007/s40565-015-0176-1.

64. J. Kim, J. M. Guerrero, P. Rodriguez, R. Teodorescu, and K. Nam, "Mode Adaptive Droop Control With Virtual Output Impedances for an Inverter-Based Flexible AC Microgrid," *IEEE Transactions on Power Electronics, IEEE,* 26, no. 3 (2011): 689–701, https://doi.org/10.1109/TPEL.2010.2091685.

65. L. Haoming, C. Yi, L. Shanshan, and H. Yunhe, "*Improved Droop Control of Isolated Microgrid with Virtual Impedance," in 2013 IEEE Power & Energy Society General Meeting* (2013), 1–5, https://doi.org/10.1109/PESMG.2013.6672849.

66. A. S. Vijay, N. Parth, S. Doolla, and M. C. Chandorkar, "An Adaptive Virtual Impedance Control for Improving Power Sharing Among Inverters in Islanded AC Microgrids," *IEEE Transactions on Smart Grid* 12, no. 4 (2021): 2991–3003, https://doi.org/10.1109/TSG.2021.3062391.

67. Y. Batmani, Y. Khayat, S. Najafi, and J. M. Guerrero, "Optimal Integrated Inner Controller Design in AC Microgrids," *IEEE Transactions on Power Electronics* 37, no. 9 (2022): 10372–10383, https://doi.org/10.1109/TPEL.2022.3165355.

68. A. Saim, R. Mellah, A. Houari, M. Machmoum, and A. Djerioui, "Adaptive Resonant Based Multiloop Control Strategy for Parallel Distributed Generation Units in Stand-Alone Microgrid Application,"

Electric Power Systems Research 143 (2017): 262–271, https://doi.org/10.1016/j.epsr.2016.10.010.

69. X. Li, P. Lin, Y. Tang, and K. Wang, "Stability Design of Single-Loop Voltage Control With Enhanced Dynamic for Voltage-Source Converters With a Low LC-Resonant-Frequency," *IEEE Transactions on Power Electronics* 33, no. 11 (2018): 9937–9951, https://doi.org/10.1109/TPEL.2018.2794066.

70. J. Hu, Y. Shan, J. M. Guerrero, A. Ioinovici, K. W. Chan, and J. Rodriguez, "Model Predictive Control of Microgrids – An Overview," *Renewable and Sustainable Energy Reviews* 136 (2021): 110422, https://doi.org/10.1016/j.rser.2020.110422.

71. V. Rajakumar, K. Anbukumar, and A. I.Selwynraj, "Sliding Mode Controller-Based Voltage Source Inverter for Power Quality Improvement in Microgrid," *IET Renewable Power Generation* 14, no. 11 (2020): 1860–1872, https://doi.org/10.1049/iet-rpg.2019.1305.

72. Y. Liao and X. Wang, *Evaluation of Voltage Regulators for Dual-Loop Control of Voltage-Controlled VSCs," IEEE, in 2019 IEEE Energy Conversion Congress and Exposition (ECCE)* (2019), 5036–5042, https://doi.org/10.1109/ECCE.2019.8912561.

73. C. A. Hammouda, R. Bradai, R. Boukenoui, A. Kherbachi, and A. Bendib, "Modeling and Design of Primary Control's Inner Loops for Droop-Controlled Three-Phase Inverters Within a Microgrid System," in *2023 International Conference on Advances in Electronics, Control and Communication Systems* (ICAECCS) (IEEE, 2023), 1–6, https://doi.org/10.1109/ICAECCS56710.2023.10105047.

74. M. Castilla, L. G. de Vicuña, and J. Miret, "Control of Power Converters in AC Microgrids," in Microgrids Design and Implementation, eds. A. C. Zambroni de Souza and M. Castilla (Springer Verlag, 2019), 139–170.

75. C. A. Hammouda, R. Bradai, A. Kherbachi, A. Bendib, R. Boukenoui, and K. Kara, "ESOGI-Based Virtual Impedance Control Scheme with Performance Improvement for Droop-Operated Three-Phase VSIs in Islanded AC Microgrid," in *2023 1st International Conference on Renewable Solutions for Ecosystems: Towards a Sustainable Energy Transition (ICRSEtoSET)* (IEEE, 2023), 1–6, https://doi.org/10.1109/ICRSEtoSET56772.2023.10525370.

76. D. Dong, B. Wen, D. Boroyevich, P. Mattavelli, and Y. Xue, "Analysis of Phase-Locked Loop Low-Frequency Stability in Three-Phase Grid-Connected Power Converters Considering Impedance Interactions," *IEEE Transactions on Industrial Electronics* 62, no. 1 (2015): 310–321, https://doi.org/10.1109/TIE.2014.2334665.

77. A. Bendib, A. Kherbachi, A. Chouder, H. Ahmed, and K. Kara, "Advanced Control Scheme and Dynamic Phasor Modelling of Grid-Tied Droop-Controlled Inverters," *IET Renewable Power Generation*, 19, no. 1 (2025): e12610.https://doi.org/10.1049/rpg2.12610.

78. A. Bendib, A. Chouder, K. Kara, A. Kherbachi, S. Barkat, and W. Issa, "New Modeling Approach of Secondary Control Layer for Autonomous Single-Phase Microgrids," *Journal of the Franklin Institute* 356, no. 13 (2019): 6842–6874, https://doi.org/10.1016/j.jfranklin.2019.04.020.